Stem Cell Research & Therapy

RESEARCH

Open Access

Identification of CD141$^+$vasculogenic precursor cells from human bone marrow and their endothelial engagement in the arteriogenesis by co-transplantation with mesenchymal stem cells

Gabee Park[1†], Dae Yeon Hwang[1†], Do Young Kim[2], Ji Young Han[1], Euiseon Lee[1], Hwakyung Hwang[1], Jeong Seop Park[2], Dae Wook Kim[1,3], Seonmin Hong[1], Sung Vin Yim[1,4], Hyun Sook Hong[2,5*] and Youngsook Son[1,3*]

Abstract

Background Critical limb ischemia (CLI) is a condition characterized by insufficient blood flow to the lower limbs, resulting in severe ischemia and potentially leading to amputation. This study aims to identify novel vasculogenic precursor cells (VPCs) in human bone marrow and evaluate their efficacy in combination with bone marrow-derived mesenchymal stem cells (BM-MSCs) for the treatment of CLI.

Methods Ex vivo cultured VPCs and BM-MSCs from bone marrow were characterized and their effects on neovascularization and long-term tissue regeneration were tested in a mouse CLI model.

Results VPCs, expressing high levels of hepatocyte growth factor and c-MET, were identified from human bone marrow aspirates. These cells exhibited strong vasculogenic capacity in vitro but possessed a cellular phenotype distinct from those of previously reported endothelial precursor cells in circulation or cord blood. They also expressed most surface markers of BM-MSCs and demonstrated multipotent differentiation ability. Screening of 376 surface markers revealed that VPCs uniquely display CD141 (thrombomodulin). CD141$^+$VPCs are present in BM aspirates as a rare population and can be expanded ex vivo with a population doubling time of approximately 20 h, generating an elaborate vascular network even under angiogenic factor-deficient conditions and recruiting BM-MSCs to the network as pericyte-like cells. Intramuscular transplantation of a combination of human CD141$^+$VPCs and BM-MSCs at a ratio of 2:1 resulted in limb salvage, blood flow recovery, and regeneration of large vessels in the femoral artery-removed CLI model, with an efficacy superior to that of singular transplantation. Importantly, large arteries and arterioles in dual cell transplantation expressed human CD31 in the intima and human α-smooth muscle actin in media layer at 4

[†]Gabee Park and Dae Yeon Hwang contributed equally to this work.

*Correspondence:
Hyun Sook Hong
hshong@khu.ac.kr
Youngsook Son
ysson@khu.ac.kr
Full list of author information is available at the end of the article

and 12 weeks, likely indicating their lineage commitment to endothelial cells and vascular smooth muscle, respectively, in vivo.

Conclusion Dual-cell therapy using BM-derived CD141$^+$ VPCs and BM-MSCs holds potential for further development in clinical trials to treat peripheral artery disease and diabetic ulcers.

Keywords Endothelial precursor cell (EPC), Vascular precursor cell (VPC), Multipotent stem cell (MSC), CD141, Thrombomodulin, Hepatocyte growth factor (HGF), Hind limb ischemia, Vascularization, Peripheral artery disease (PAD)

Background

Endothelial precursor cells (EPCs) were initially characterized by Asahara et al. [1]. EPCs isolated from the umbilical cord and peripheral blood (PB) mononuclear cells (MNCs) exhibit vasoreparative ability in vitro and in vivo but have dissimilar cellular and molecular properties [2, 3]. Early EPCs, myeloid angiogenic cells (MACs), and circulating angiogenic cells (CACs) have myeloid and hematopoietic origins; they exhibit limited proliferative potential and cannot generate tube-like structures *in vitro* but can stimulate the formation of new blood vessels by secreting angiogenic growth factors, chemokines, and cytokines rather than directly integrating into vascular networks [4]. Outgrowth endothelial cells (OECs) or endothelial colony forming cells (ECFCs), derived from adherent cells between 7 and 21 days, exhibit endothelial-lineage commitment [4, 5] but are not originated from the bone marrow [6]. Protein C receptor (CD201, also known as EPCR)-expressing endothelial cells (ECs) and CD157 (BST-1)-expressing side population cells, which were recently identified as tissue-resident vascular endothelial stem cells (VESCs) in the development of mouse mammary fat pads [7] and in the intima of large vessels of the mouse liver and other tissues, are expected to be involved in homeostatic and regenerative events or pathological disease and cancer development [2, 8]. Accordingly, mouse VESCs in the vessel intima and OECs isolated from the blood, expressing most endothelial surface markers, such as CD31, vascular endothelial (VE)-cadherin, and vascular endothelial growth factor receptor 2 (VEGFR2), may be classified as endothelial-lineage-committed tissue stem cells or activated ECs. However, human VESCs are yet to be identified, and consistent endothelial-lineage commitment efficacy of OECs is lacking. Moreover, the definitive phenotype of EPC-like or vasculogenic cells derived from a variety of tissues remains elusive, which has led to a considerable debate regarding the selection of specific surface markers.

Peripheral artery disease (PAD) refers to atherosclerosis affecting arteries of the lower extremities, which results in a sudden lack of blood flow and embolism commonly occurring in the femoral artery [9]. Clinical interventions for limb ischemia focus primarily on transient reperfusion rather than neovascularization. Numerous clinical trials have explored therapeutic neovascularization using granulocyte-colony stimulating factor or granulocyte–macrophage colony-stimulating factor-mobilized unselected MNCs [10], CD34-sorted bone marrow MNCs (BM-MNCs) [11], ex vivo cultured mesenchymal stem cells (MSCs) [12], and MSC-like cell. It is well established that adult stem cell therapies are generally safe and well tolerated, with minimal or transient side effects. However, due to variable outcomes of individual clinical studies, the efficacy of stem cell therapy remains inconclusive. Notably, consistent efficacy and long-term reparative engagement of these therapeutic cells have yet to be validated [13–15].

No evidence is available for transdifferentiation of MNCs, CD34-sorted cells, and MSCs into vascular ECs or smooth muscle cells. However, multipotent vasculogenic pericytes [16], CD34$^+$ progenitor cells [17], CD144$^+$ ECs derived from induced pluripotent stem cells (iPSCs) [18], and vascular progenitor cells (VPCs) genetically induced using Etv2 and Fli1 genes [19] were found to be effective in vascular recovery, and their engraftment as human endothelial intima and smooth muscle layer or pericytes in the capillary and artery of critical limb ischemia model (CLI) strongly supports their bipotent differentiation capacity and reparative function.

Vascular growth and remodeling depend on the generation of new ECs from stem cells or on sprouting of activated ECs. Perivascular cells, such as pericytes and smooth muscle cells, are crucial for vessel integrity and function [20]. Therefore, in cell replacement therapy for neovascularization in situ, a context-dependent acquisition of endothelial and smooth muscle cell phenotypes from multipotent progenitor cells or a combination of at least two different functional cells is definitively required rather than singular cell transplantation applied currently. Highly clonogenic cells of both cell fates for endothelial intima and smooth muscle cell media layer are required for therapeutic vascularization using ex vivo cultured cells. Currently, circulating ECFCs have limited cell expansion capacity for autologous cell therapy [21]. iPSC-derived EPCs or VPCs have safety concerns [22],

and ECFC-like cells from cord blood (CB) have immunological issues [23].

In this study, we attempted to identify highly clonogenic and vasculogenic clones from human bone marrow aspirates (BMA) collected from individuals of different ages and sex, either in frozen stocks of MNCs from BMA or fresh BMA, primarily using adherent phenotype and specific culture media. These vasculogenic cells were compared using surface marker screening, secretome, Matrigel tube formation, and population doubling time (PDT) with those from peripheral or cord blood, as well as with those from bone marrow-derived mesenchymal stem cell (BM-MSC) culture. These novel cells were multipotent, expressed CD141 (thrombomodulin) unlike BM-MSCs, yielded 2×10^{10} cells within 3 weeks from 1×10^{7} BM-MNCs with ~ 20 h PDT, and could recruit BM-MSCs to the vascular tube similar to pericytes, which was newly named as $CD141^{+}$VPCs. A combination of $CD141^{+}$VPCs and BM-MSCs was applied to the CLI model of nude mice, and limb salvage and cell fates in vivo were compared with those in singular transplantation to assess their preclinical efficacy.

Methods

Cell culture

For primary culture of BM-VPCs and BM-MSCs, BM-MNCs were purchased from STEMCELL Technologies (#70,001, Vancouver, Canada) and Lonza (#2M-125C, Basel, Switzerland). In addition, BM-MNCs were isolated from fresh BM using density gradient separation. Fresh BM was obtained from donors (with approval from the Institutional Review Board; approval number: 2020-09-036) or purchased from CGT Global (Folsom, CA). Details and demographics of donor information were listed (Additional file 1: Table S1). BM-MNCs were plated at a density of $3–15\times10^{6}$ cells/T-75 flask pre-coated with Humatein (Rokit healthcare, South Korea) and cultured with EGMPL media for BM-VPC culture or plated in a non-coated T-75 flask with StemMACS media for BM-MSC culture, respectively (Additional file 1: Figure S1). EGMPL is an abbreviation for FBS-depleted EGM-2 (Lonza) medium with 2% human platelet lysate (hPL, PL Bioscience) and 2 IU/ml heparin (JW Pharmaceutical, Gwacheon, South Korea). StemMACS is an abbreviation for StemMACS MSC expansion medium XF, human (Miltenyi Biotec, Bergisch Gladbach, Germany). The cells were incubated at 37 °C in a 5% CO_2 atmosphere. The medium was changed once every 2–3 days. The first subculture was conducted 9–11 days after seeding when the colonies were almost confluent. After passage 1, the cells were sub-cultured at 70–90% confluency. In every subculture, cells were counted by Acridine Orange/Propidium Iodide staining using a LUNA FX7 automatic cell counter (Logos Biosystems, Anyang, South Korea). Cell yield and PDT were calculated based on cell counting.

Flow cytometry

Flow cytometry was performed to characterize the cluster of differentiation (CD) markers of BM-VPCs, BM-MSCs, CB-endothelial colony forming cells (ECFCs), PB-ECFCs, and human umbilical cord vein endothelial cells (HUVECs). Cells were incubated with Alexa Flour 647-conjugated c-MET (R&D systems, Minneapolis, MN), Alexa Flour 488-conjugated von Willebrand Factor (vWF, Abcam, Cambridge, MA), fluorescein-labeled UEA-1 (Ulex europaeus agglutinin-1, Vectorlabs, Burlingame, CA), allophycocyanin (APC)-conjugated anti-CD29, CD31, CD34, CD44, CD45, CD73, CD90, CD105, CD141, CD282, and CD309 antibody (Miltenyl Biotec, Bergisch Gladbach, Germany) or an isotype control conjugated to APC (Miltenyi Biotec), Alexa Fluor 647 (R&D systems) and Alexa Fluor 488 (Abcam). The cells were analyzed using a NovoCyte 3000 flow cytometer (Agilent Technologies, Santa Clara, CA) and NovoExpress software. To analyze the induction of endothelial cell markers of BM-VPCs while undergoing the tube formation, PKH67 (Sigma-Aldrich) green-labeled BM-VPCs, and unlabeled BM-MSCs or HUVECs were used to distinguish BM-VPCs from BM-MSCs or HUVECs. BM-VPCs were re-suspended with various assay media (MEM-α + 0.2%hPL with or without 500 pg/mL TNF-α and EGM-2). BM-VPCs and BM-MSCs were mixed at a ratio of 2:1 in MEM-α + 0.2%hPL medium with or without 500 pg/mL tumor necrosis factor-α (TNF-α, R&D system). BM-VPCs and HUVECs were mixed at a ratio of 1:1 using MEM-α + 0.2%hPL and EGM-2 medium and seeded on Matrigel at a density of 1.5×10^{4} cells/well for 27 h to give sufficient time for protein expression. For flow cytometry, the tube on Matrigel was dissociated into single cell by the CTS™ TrypLE™ enzyme (Gibco). PKH-green positive BM-VPCs and PKH-green negative BM-MSCs or HUVECs were gated to analyze CD31, CD309, and CD144 expression of each cell. After gating, APC-conjugated CD31, CD309, and CD144 were analyzed.

In vitro Matrigel tube formation assay

Growth factor-reduced Matrigel (Corning, NY, USA) was aliquoted at 10 µl per well in µ-slide (Ibidi, Grafelfing, Germany) and incubated at 37 °C for 30 min for gelation. Then, a mixture of BM-VPCs and BM-MSCs at different cell ratios, PB-ECFCs, CB-ECFCs, and HUVECs were resuspended either in MEM-α supplemented with 0.2% hPL or EGM-2 media and total cell numbers of 6×10^{3} at each cell combination were seeded on the Matrigel in each well. For the tube formation assay in an inflammatory environment, 500 pg/ml TNF-α was added to the

MEM-α medium with 0.2% hPL. At 16–18 h of incubation, vessel structures were observed using phase contrast microscopy (Nikon, Olympus), and the total tube length, total master segment length, number of meshes, number of master segments, and number of isolated segments were determined using the angiogenesis analyzer in the Image J software (NIH, MD, USA).

Immunofluorescence staining

For immunofluorescence staining, BM-VPCs and BM-MSCs were cultured on coverslips. The cells were fixed with 3.7% formaldehyde (Sigma-Aldrich MO) and permeabilized with 0.2% Triton X-100 buffer (Sigma-Aldrich) for 10 min at room temperature (RT). For blocking, the cells were incubated with 20% normal goat serum for 1 h at RT and then, treated with primary antibodies overnight to detect CD141 (Abcam, ab109189; 1:100) and α-SMA (Abcam, ab5694; 1:100) at 4 °C, with Alexa Fluor 488- or 568-conjugated secondary antibodies (Invitrogen, Waltham, Massachusetts; 1:1000) for 1 h at RT, and mounted with a mounting medium with DAPI (Vector Laboratories, Burlingame, CA) for nuclear staining. Cell images were obtained using a fluorescence microscope (Leica, Wetzlar, Germany).

Animal experiments

Male BALB/c nu mice (five-week-old, 18–20 g) were used to avoid complication associated with hormonal cycles in females which may affect angiogenic event, purchased from DBL (Daejeon, South Korea), housed under a 12 h light/dark cycle in an SPF animal room, and allowed to acclimatize for 7 days before experiments. This study was approved by the Ethics Committee for Experimental Animals of Kyung Hee University Hospital (approval number: KHMC-IACUC 20-008). The work has been reported in line with the ARRIVE guidelines 2.0.

Induction of CLI in nude mice

Before surgery, the mice were anesthetized via an intraperitoneal injection of a combination of ketamine (75 mg/kg; Yuhan, Seoul, Korea) and rompun (1.2 mg/kg; Bayer Healthcare, Kyunggi-do, Korea). Following an incision from the ankle to below the abdomen, the common femoral artery and nerve were meticulously exposed and dissected from artery to nerve. The upper common femoral artery was ligated using 6–0 silk (1st ligation). Additionally, two points along the superficial femoral artery, one distal and the other proximal, were ligated using 6–0 silk sutures. Subsequently, a segment of the superficial femoral artery between the 2nd and 3rd ligated sites was excised (Additional file 1: Figure S2), and blood flow was assessed using a Laser Doppler blood flow imager (OMEGAZONE OZ-2, Tokyo, Japan). Mice with blood flow rates < 40% were selected for cell transplantation. For analysis, all mice were euthanized with CO_2 (3 L/min), followed by bilateral thoracotomy.

Cell transplantation

Human BM-VPCs and BM-MSCs (1.2×10^5/50 μl per mouse) were prepared for transplantation at passage 3. BM-VPCs only (1.2×10^5/50 μl), BM-MSC only (1.2×10^5/50 μl) or a combination of BM-VPCs (8×10^4/25 μl) and BM-MSC (4×10^4/25 μl) was suspended in saline. The cell suspension (50 μl) was then transferred to the insulin syringe (a 28G, 0.5 cc needle) and slowly injected to the CLI-induced muscle at five sites, with an injection depth of approximately 1.5 mm (10 μl/site). Two applications were made below the first ligation, carefully avoiding fat tissue, while three were administered between the second and third ligation, in the area where the artery was removed. The injections were administered along both sides of the femoral artery, 2 mm away from the nerve and artery, with an interval of approximately 4–6 mm between injections (Additional file 1: Figure S2).

Evaluation of ischemic score

Ischemic necrosis at the injury site was assessed by monitoring physiological changes, including skin discoloration, swelling, and advancement of ischemic damage (Additional file 1: Figure S3). The severity of ischemic necrosis in the injured leg was graded on a scale of 7 based on the extent of ischemia: Grade 0, limb salvage; Grade 1, swelling, discoloration, and nail necrosis; Grade 2, toe with little necrosis; Grade 3, toe with severe necrosis (necrosis extending to the walking pad of the foot); Grade 4, foot necrosis; Grade 5, knee necrosis; and Grade 6, limb loss. The ischemic necrosis grade was independently assessed by three observers (blind test) on postoperative days 1, 2, 3, 7, 14, and 28.

Blood flow analysis

Mice were anesthetized to minimize pain-induced fluctuations. After confirming regular heartbeats, blood flow in the ischemic leg of mice was measured using a laser Doppler blood flow imager (OMEGAZONE OZ-2), while the temperature was consistently maintained by keeping the mouse warm throughout the surgery. Blood flow in both legs was measured following the induction of hind limb ischemia (day 0), and subsequently on days 7, 14, and 28. Measurements of blood flow were taken over a period to counteract temperature-affected rapid changes in blood flow. Multiple blood flow images were acquired and analyzed. Blood flow was quantified using the LIA 4.2 software, with blood flow values calculated as a ratio between the ischemic and non-ischemic legs.

Immunohistochemistry staining

Hind limb muscles were harvested at 28 days post induction, fixed in 3.7% formaldehyde (Sigma-Aldrich), and processed using a TP1020 tissue processor (Leica Biosystems, Wetzlar, Germany). The areas where the femoral artery was excised (between the 2nd and 3rd ligated sites) were analyzed. The samples were rehydrated with serially graded ethanol, boiled with 0.01 M sodium citrate (Sigma-Aldrich) for antigen retrieval, treated with 0.01% sodium borohydride (Sigma-Aldrich) to reduce background autofluorescence, and permeabilized using 0.3% Triton X-100. The samples were blocked with 2% normal goat serum (Vector Laboratories, INC., Newark, CA), incubated overnight with primary antibodies to detect CD31, α-SMA, and transgelin (TAGLN, Abcam, Cambridge, UK) at 4 °C, incubated with alkaline phosphatase-conjugated secondary antibodies, fluorescein (FITC)-labeled secondary antibodies (Vector Laboratories, INC.) or Cy3-conjugated secondary antibodies (The Jackson Laboratory, Bar Harbor, Maine), and subsequently, incubated with Alexa-488 or Alexa 594-conjugated WGA (Invitrogen, Waltham, Massachusetts; 1:200). Color development was performed using Vector® Blue Substrate Kit. Nuclei were counterstained using 4′,6-diamidino-2-phenylindole (DAPI, Sigma-Aldrich, 1:1000) or fast red (Vector Laboratories). Images were acquired using a Carl Zeiss confocal microscope (Oberkochen, Germany) and analyzed using the ZEN Microscopy software (Carl Zeiss).

Western blot analysis

Cell or tissue extracts were prepared using a lysis buffer (Cell Signaling Technology, Danvers, Massachusetts) containing 2 mM phenylmethylsulfonyl fluoride (PMSF, Sigma Aldrich). The insoluble fraction was discarded by centrifugation at 14,000×*g* at 4 °C for 10 min. Protein concentrations were determined using the bicinchoninic acid reagent (Thermo Fisher Scientific). Protein lysates (10ug for cell lysate and 150ug for tissue homogenate) were separated using sodium dodecyl sulfate–polyacrylamide gel electrophoresis and transferred onto a nitrocellulose membrane. Membranes were blocked with 5% skim milk in TBS-T for 1 h at RT. Thereafter, the membranes were incubated with primary antibodies to detect CD31 (Abcam, ab134168; 1:1000), CD141 (Abcam, ab109189; 1:1,000), α-SMA (Abcam, ab5694; 1:400), c-MET (Cell Signaling Technology, 8198; 1:1000), Transgelin (Abcam, ab14106; 1:1000), GAPDH (Abcam, ab181602; 1:10,000), and α-tubulin (Sigma-Aldrich, T-5168; 1:4000) at 4 °C overnight, incubated with anti-immunoglobulin G horseradish peroxidase-conjugated secondary antibody for 1 h at RT, and visualized using EZ-Western Lumi Pico (Dogen, Seoul, Korea).

Statistical analysis

Data are presented as mean ± standard deviation (SD) of values from three independent experiments. To confirm statistical significance, a one-way analysis or kruskawallis with Tukey's multiple comparisons or Dunnett's or Dunn's test (post-hoc test) or t-test was performed. The statistical analyses applied in each experiment were described in the respective figure legends. Significance levels are indicated as follows: $^{*}p < 0.05$, $^{**}p < 0.01$, and $^{***}p < 0.001$.

Results

Identification of highly clonogenic and vasculogenic precursor cells, distinct from peripheral blood or cord blood-derived ECFCs, from human BMA

Candidate VPCs with high clonogenic capacity were identified in the Endothelial Growth Medium culture of MNCs from human BMA. These BM-derived VPCs (BM-VPCs) generated a vascular network on Matrigel but did not express conventional surface markers of EPC-like or activated ECs, such as CD31 (PECAM-1), CD133 (prominin-1), CD144 (VE-cadherin), and CD309 (KDR/Flk-1/VEGFR2), reported in PB and CB (Additional file 1: Figure S4). These BM-VPCs were also distinct from MSC-like cells in terms of vasculogenic capacity but could cooperate with each other for complex vascular network formation on Matrigel.

To develop BM-VPCs for use in autologous vascular cell therapy, they were further characterized and their expansion efficiency was optimized (Fig. 1A–C). BM-VPCs were best cultured in the fetal bovine serum (FBS)-depleted EGM2 supplemented with 2% hPL

(See figure on next page.)

Fig. 1 Identification of VPCs, distinct from PB and CB-derived ECFCs, from BM. **A** Morphology of BM-VPCs, PB-ECFCs, CB-ECFCs in passages 0 and 3. Colonies were formed from mononuclear cells derived from the BM, PB, and CB. Scale bar = 500 μm. **B, C** Cell yield and PDT of CB-ECFCs, PB-ECFCs, and BM-VPCs (cell yield data of BM-VPCs presented as mean ± SD, n = 39). **D** Images showing the results of in vitro Matrigel tube formation assay for BM-VPCs, HUVECs, CB-ECFCs, and PB-ECFCs in the EGM-2 medium containing VEGF, EGF, FGF, IGF, and other growth factors, and in the MEMα + 0.2%hPL (lacking angiogenic growth factors). After overnight incubation, the morphology of tubes was observed using a phase contrast microscope. Scale bar = 500 μm. **E** UEA-1 binding ability of cells at passage 5 tested using flow cytometry. **F** Expression of markers of EPCs and MSCs in HUVECs, CB-ECFCs, PB-ECFCs, BM-VPCs, and BM-MSCs, analyzed using flow cytometry at passage 5

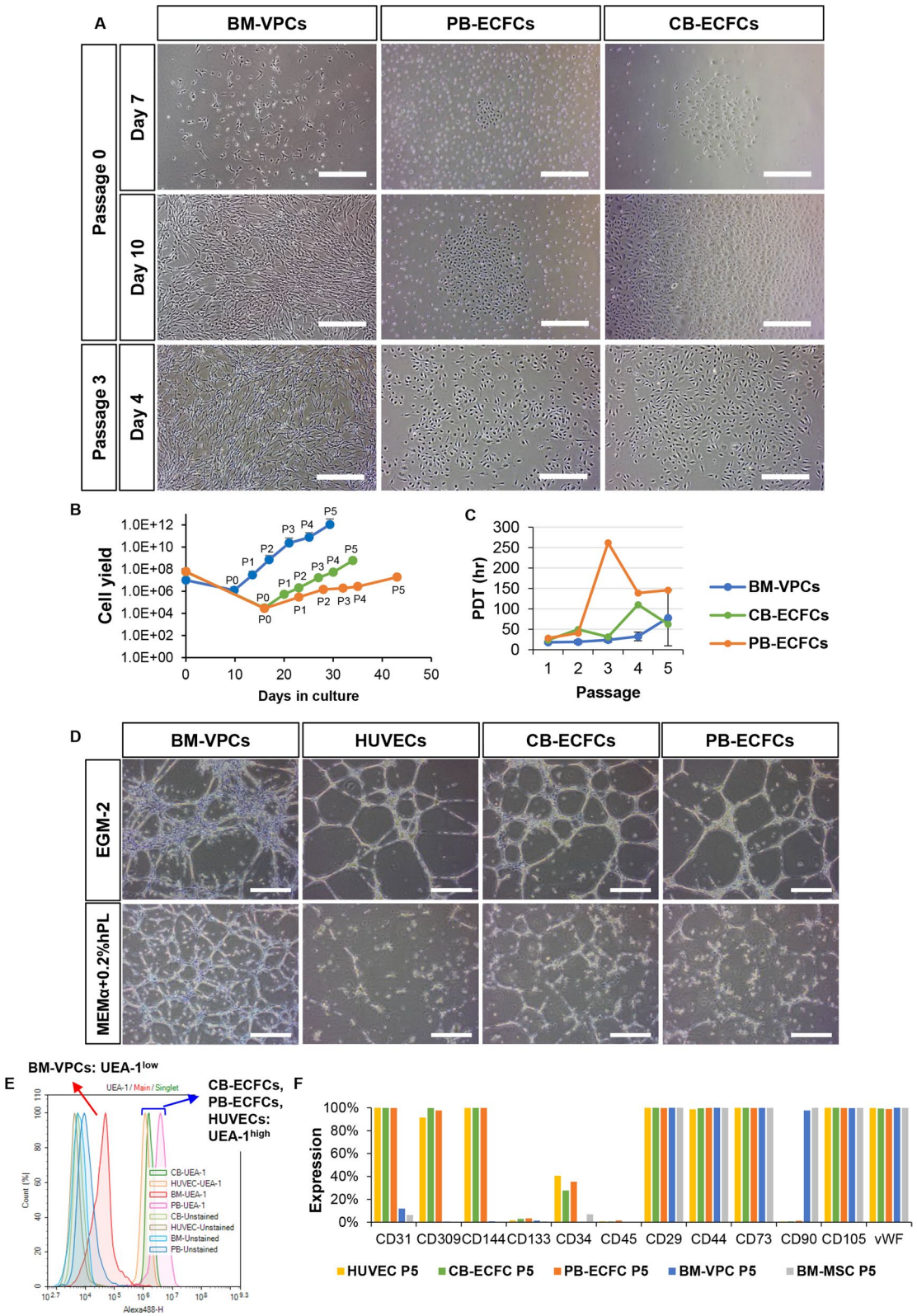

Fig. 1 (See legend on previous page.)

(EGMPL) (Additional file 1: Figure S4). In the culture of BM-MNCs from 32 donors, the initial spindle-shaped colonies became apparent by day 4 and could be expanded over a three-week culture period, with a PDT of ~ 20 h (passage 3) (Fig. 1A). This cell expansion capacity yielded ~ 20 billion cells, starting with 10 million BM-MNCs (Fig. 1B, C, and Additional file 1: Table S1-3). The clonogenic capacity and cellular characteristics of BM-VPCs were compared with those of PB-ECFCs and CB-ECFCs, derived from EGM-2 cultures of PB and CB, respectively. These cells exhibited cobblestone morphology, similar to that of activated ECs, such as HUVECs, and formed initial colonies on days 7–10 (Fig. 1A). Because the PDT of these cells was much longer (by ~ 5.5- and 1.7-fold (passage 1–3 average), for PB-ECFCs and CB-ECFCs, respectively) than that of BM-VPCs, they cannot meet the cell expansion efficiency required for vascular therapeutics (Fig. 1B, C, Additional file 1: Table S2).

To determine vasculogenic capacity, we examined in vitro vessel formation on Matrigel (Fig. 1D). PB-ECFCs, CB-ECFCs, and HUVECs, used as a positive control for activated ECs, formed a good vascular network in EGM-2 medium supplemented with a variety of angiogenic factors, such as basic-fibroblast growth factor (FGF), vascular endothelial growth factor (VEGF), epidermal growth factor (EGF), and R3-insulin-like growth factor (IGF). However, HUVECs failed to form a vascular network and PB-ECFCs and CB-ECFCs generated rather disrupted vascular structures in the MEMα + 0.2%hPL medium deficient in angiogenic factors, highlighting the essential requirement of angiogenic factors. However, BM-VPCs formed huge and thick meshes in the EGM-2 medium and several small vascular meshes in the MEMα + 0.2%hPL medium (Fig. 1D, Additional file 1: Figure S5), which indicated its vasculogenic capacity even under angiogenic factor-deficient condition.

Next, we examined the fluorescein-labeled UEA1-binding ability of the cells, a criterion for mature ECs, using flow cytometry. HUVECs, CB-ECFCs, and PB-ECFCs were shifted to UEA-1^{high} whereas BM-VPCs were shifted to UEA-1^{low} (Fig. 1E). CD45 and CD133 were not expressed in any of the tested cells. CD34, an hematopoietic stem cell (HSC) lineage marker, was not expressed in BM-VPCs and BM-MSCs but partially expressed in HUVECs, CB-ECFCs, and PB-ECFCs. vWF, an EC marker, was expressed in all cells, including BM-MSCs. EC markers, such as CD31, CD309, and CD144, were not expressed in BM-VPCs and BM-MSCs but expressed in over > 90% of HUVECs, CB-ECFCs, and PB-ECFCs, strongly suggesting that PB-ECFCs and CB-ECFCs may be similar to activated ECs. The characteristic MSC markers, such as CD29, CD44, CD73, and CD105, were expressed in all cells but CD90 was expressed only in BM-VPCs and BM-MSCs (Fig. 1F). Overall, in terms of the expression of surface markers and cell morphology, BM-VPCs did not exhibit the cellular phenotype of ECs or ECFCs but were autonomously vasculogenic in vitro.

BM-VPCs can recruit BM-MSCs to form a stable vascular network even in the presence of TNF-α

BM-VPCs exhibited a phenotype most similar to that of MSCs rather than ECs but retained a strong vasculogenic capacity even under angiogenic factor-deficient conditions. Previously, BM-MSCs were reported to differentiate into vascular smooth muscle cells [24] and pericytes in a reconstruction of blood–brain barrier on a chip [25]. We, therefore, compared the vasculogenic capacities of BM-VPCs, BM-MSCs, and their combination using the Matrigel tube formation assay in MEMα + 0.2%hPL wherein BM-VPCs and BM-MSCs were used at different ratios (Fig. 2A). BM-VPCs-only (1:0) formed a good

(See figure on next page.)

Fig. 2 Vasculogenic capacity of BM-VPCs and their cooperation with BM-MSCs and HUVECs in Matrigel tube formation. **A** Comparison of the in vitro tube-forming ability of various combinations of BM-VPCs and BM-MSCs. Scale bar = 500 μm. **B** Quantitative analysis of in vitro tube formation. Different parameters were measured using an angiogenesis analyzer in the Image J software. Values are mean ± SD (*$p < 0.05$, **$p < 0.01$, ***$p < 0.001$, compared with 1:0, one-way ANOVA test followed by Turkey's multiple comparison test, n = 4). **C** Images showing the results of Matrigel tube formation assay conducted using PKH green-labeled BM-VPCs and PKH red-labeled BM-MSCs. Pericyte-like localization of BM-MSCs in tubular networks formed by BM-VPCs is indicated with yellow arrowheads. Junctional points of the network tightened by BM-MSCs are indicated with white dotted lines. White scale bar = 200 μm, Yellow scale bar = 100 μm. **D** Images showing the results of in vitro tube formation assay conducted under conditions mimicking an inflammatory environment by adding 500 pg/mL TNF-α in MEMα + 0.2%hPL. Scale bar = 500 μm. **E** Quantitative analysis of panel D. Different parameters were measured using an angiogenesis analyzer in the Image J software. Values are mean ± SD (*$p < 0.05$, **$p < 0.01$, ***$p < 0.001$, one-way ANOVA test followed by Turkey's multiple comparison test, n = 5). **F** Images showing the results of Matrigel tube formation assay conducted using PKH green-labeled HUVECs and PKH red-labeled BM-VPCs and BM-MSCs. HUVECs only group included 6,000 cells/well and combination groups included 3,000 (HUVECs) + 3,000 (BM-VPCs or BM-MSCs) cells /well (1:1). Scale bar = 500 μm. **G** Flow cytometry analysis of CD31 expression of PKH-green labeled BM-VPCs and unlabeled BM-MSCs before and after the tube formation in MEMα + 0.2%hPL with or without 500 pg/mL TNF-α supplementation for 27 h. **H** Flow cytometry analysis of CD31 expression of PKH-green labeled BM-VPCs after the hybrid tube formation with unlabeled HUVECs in MEMα + 0.2% hPL media or EGM-2 media for 27 h

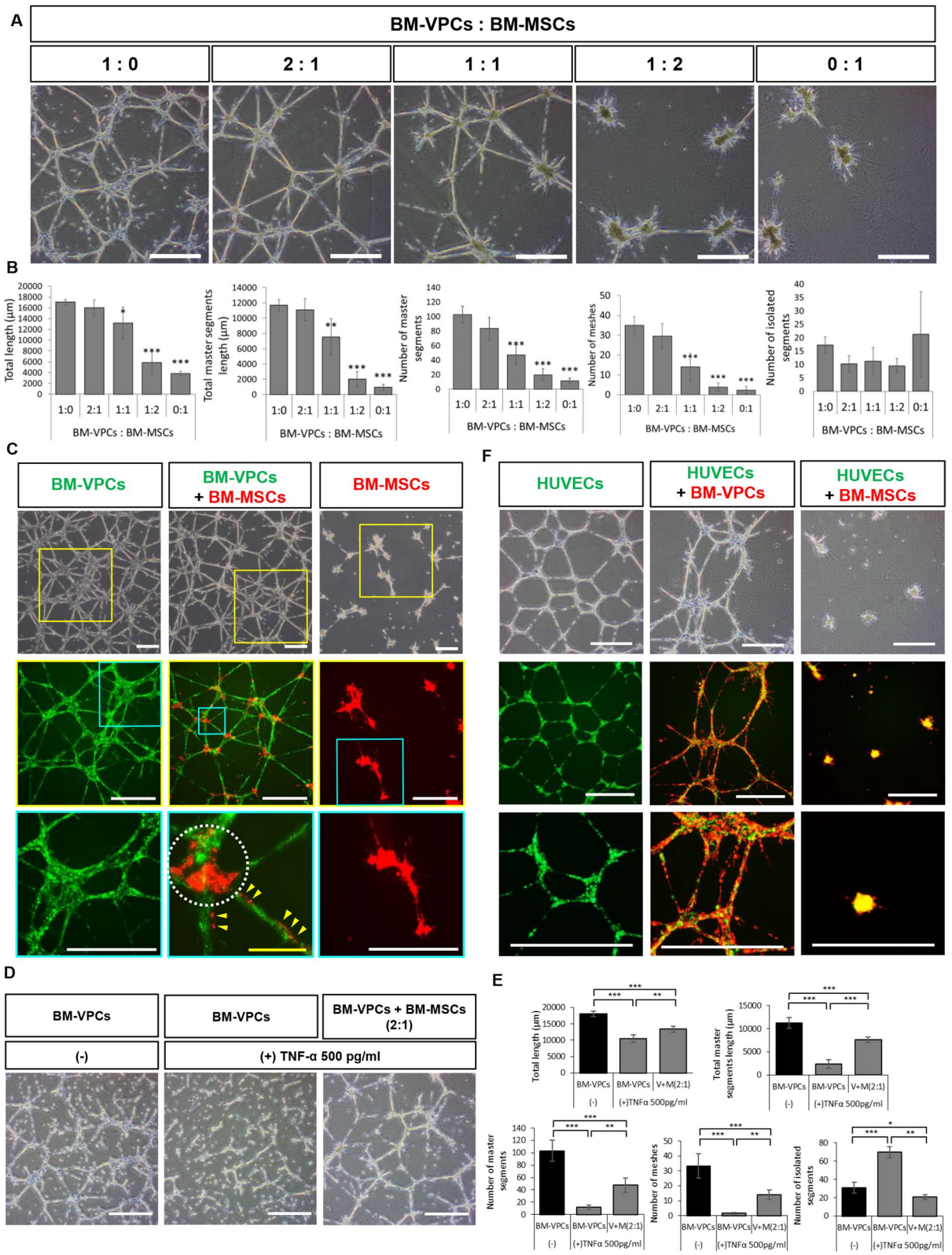

Fig. 2 (See legend on previous page.)

G

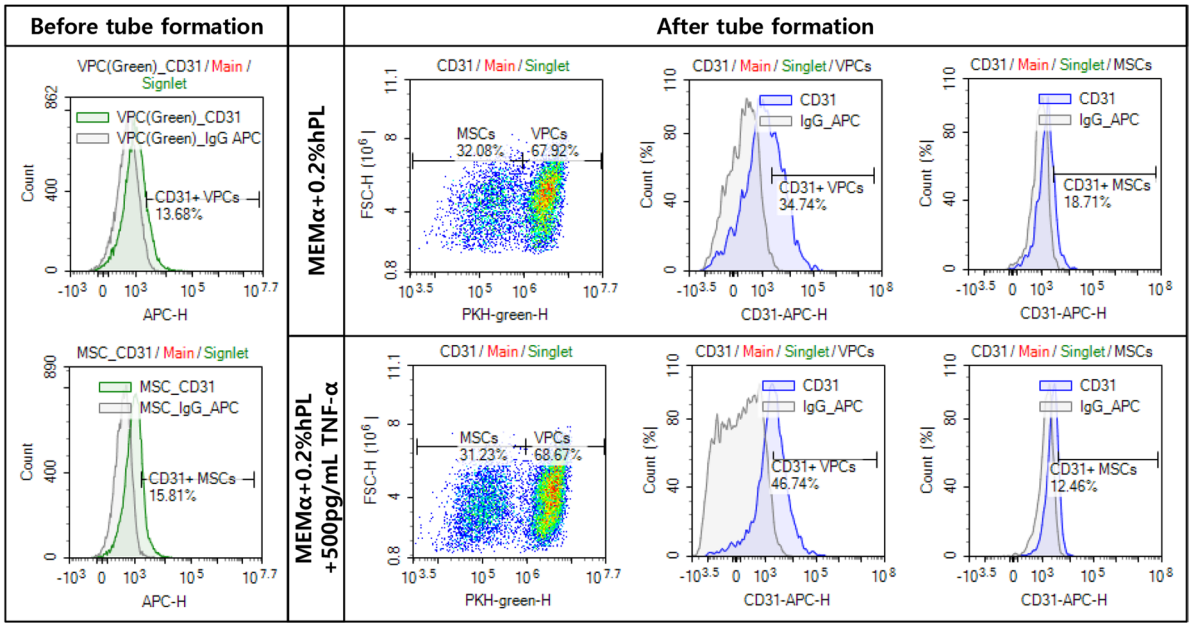

H

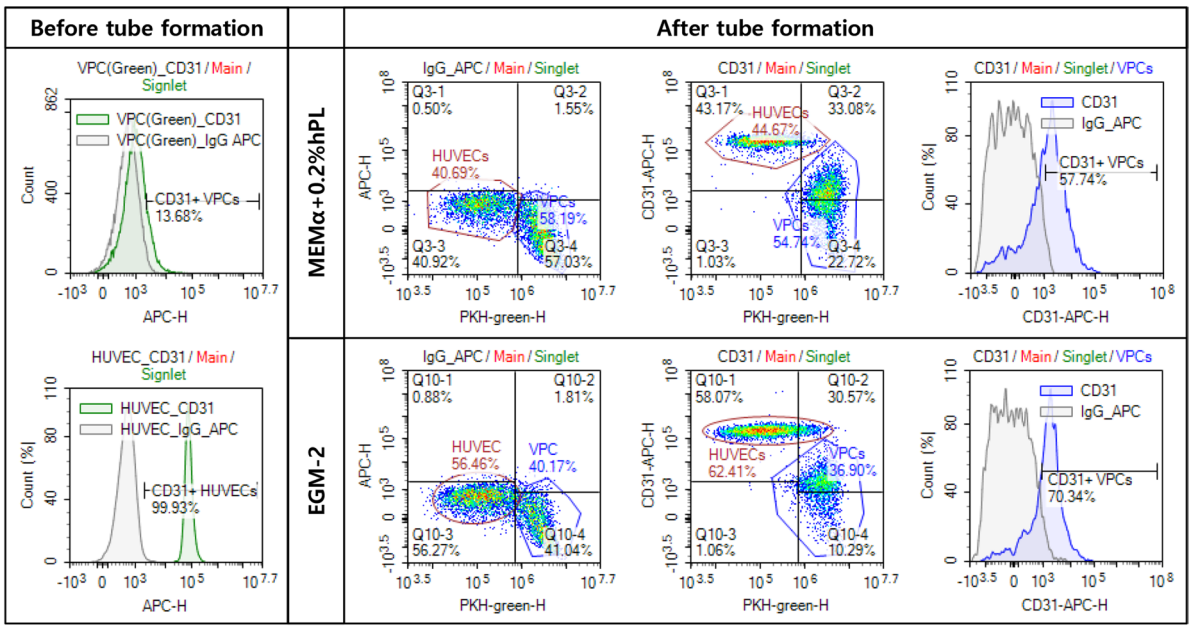

Fig. 2 continued

vascular network, whereas BM-MSC-only (0:1) did not. However, a 2:1 combination of BM-VPCs and BM-MSCs recruited most BM-MSCs to the vascular network similar to vascular pericytes. In contrast, a 1:2 combination of BM-VPCs and BM-MSCs failed to form a vascular network, and a 1:1 combination partially disrupted the vascular network. Quantitatively, the number of isolated segments, an indicator of immature vessels, was lower in the combination of BM-VPCs and BM-MSCs (2:1) than in BM-VPCs-only (Fig. 2B), suggesting the possible role of BM-MSCs as vascular pericytes in endothelial tube maturation.

To visualize the interaction and localization of BM-MSCs in the vascular network of BM-VPCs, PKH green-labeled

BM-VPCs and PKH red-labeled BM-MSCs were seeded on Matrigel (Fig. 2C). BM-MSCs is mostly localized to the junction of meshes formed by BM-VPCs, possibly stabilizing the junctional complex, but some were located on the abluminal surface of the BM-VPCs-vascular tubes, similar to vascular pericytes. Accordingly, BM-MSCs are apparently recruited to the network of BM-VPCs as vascular pericyte-like cells to tighten the vascular junction and stabilize the vascular tube by encircling the luminal side of the tube.

In the treatment of ischemic vascular diseases, most therapeutic cells may encounter inflammation at ischemic loci. To simulate the inflammatory environment, we supplemented TNF-α in the Matrigel tube assay (Fig. 2D). BM-VPCs alone formed a disrupted vascular network but a 2:1 combination of BM-VPCs and BM-MSCs maintained stable vascular networks even under TNF-α-supplemented conditions. Tubular structure was quantified (Fig. 2E). Because cell numbers and proliferation may affect the vascular network formation, the effect of TNF-α on cell viability and proliferation was tested (Additional file 1: Figure S6). TNF-α increased the viability of BM-VPCs in a dose-dependent manner, suggesting that TNF-α-mediated cytotoxicity of BM-VPCs is not involved in the disruption of vascular network even though TNF-α decreased the viability of BM-MSCs at high concentrations. Thus, BM-VPCs may survive well and retain their vasculogenic capacity even under inflammatory conditions only if BM-MSCs are co-transplanted, suggesting BM-MSCs' role on vascular stabilization like pericytes under inflammatory condition.

BM-VPCs and HUVECs can cooperate to form a large vascular network

Upon transplantation, BM-VPCs may recruit endogenous ECs to cooperate in vascular repair or may be invited to arteriogenesis through bridging collaterals. To test this possibility, PKH green-labeled HUVECs were seeded at the lower cell density, which is insufficient for massive network formation, along with PKH red-labeled BM-VPCs or BM-MSCs for Matrigel tube assay (Fig. 2F). When seeded together at a 1:1 ratio, BM-VPCs and HUVECs formed segments of large vessel-like structures composed of both cells, but HUVECs and BM-MSCs could not. BM-MSCs themselves did not retain their vasculogenic capacity. Thus, BM-VPCs may collaborate with endogenous ECs present in the injury area to regenerate new vessels.

BM-VPC stimulates CD31 expression during tube formation when supplemented with TNF-α and cocultured with BM-MSC or HUVEC

In order to explore whether BM-VPCs can induce mature endothelial markers such as CD31, VEGFR2, and VE-cadherin during tube formation under inflammatory microenvironment, CD31 expression of BM-VPCs and BM-MSCs was analyzed by flow cytometry before and after the tube formation in the presence of TNF-α. PKH-green-labeled BM-VPCs in the tube was dissociated and separated by flow cytometry gating. The cell ratio of 2:1 in a combination of BM-VPCs and BM-MSCs was fairly well maintained even after the tube formation for 27 h (Fig. 2G). Only BM-VPCs increased CD31 expressing cells from 13.68% before the tube formation to 34.07% after tube formation in MEM-α + 0.2%hPL media and furthermore to 46.74% after tube formation in the presence of TNF-α, which was not accompanied in BM-MSCs. Also, the hybrid tubes with PKH-green labeled BM-VPCs and unlabeled-HUVECs at a ratio of 1:1 as shown in Fig. 2F were allowed to form in either MEM-α + 0.2%hPL (proangiogenic factor-deficient) or EGM-2 medium (proangiogenic factors sufficient) (Fig. 2H). CD31-expressing cells in BM-VPCs was increased from 13.68 to 57.74% in MEMa + 0.2%hPL media after the tube formation and furthermore to 70.34% in EGM-2 media. However, induction of CD309(VEGFR2) and CD144(VE-cadherin) was not accompanied under the same condition (Additional file 1: Figure S7). Even though the best condition for endothelial differentiation of BM-VPCs in vitro was not identified, BM-VPC's plasticity toward endothelial cells, which is distinct from that of BM-MSC, was noted in the presence of TNF-a, BM-MSC, and HUVEC.

BM-VPCs highly express CD141, thrombomodulin, as a unique marker distinct from BM-MSCs

To distinguish between BM-VPCs and BM-MSCs, we screened 376 surface markers (Additional file 1: Figure S8). The expression of seven markers, namely CD141, CD157, CD197, CD282, CLEC4D, ROR1, and TGF-βRII, differed by more than 50% between the two cells (Fig. 3A). The expression of CD141 and CD282, which are expressed in ECs and are involved in vasculogenesis [26–28], was verified in passage 3 BM-VPCs and BM-MSCs derived from to 15–20 donors using flow cytometry (Fig. 3B). CD141 (thrombomodulin) was expressed in 73–98% of the BM-VPCs population but was barely expressed in BM-MSCs. CD282 was expressed in 2–100% of the BM-VPCs population, with large variations between donors, but was most not expressed in BM-MSCs. Thus, CD141 may be the most suitable marker for distinguishing BM-VPCs from BM-MSCs.

$CD141^{+}$BM-VPCs preexist in the bone marrow and can preferentially be expanded under specific culture conditions

To check whether CD141-expressing BM-VPCs preexist in the BM or are induced in specific ex vivo culture, CD141-positive cells were sorted from whole BM-MNCs

A

	BM-VPCs	BM-MSCs	Difference
CD141	98.67%	5.36%	93.31%
CD157	20.46%	75.74%	55.28%
CD197	34.82%	94.24%	59.42%
CD282	60.24%	4.83%	55.41%
CLEC4D	75.98%	7.03%	68.95%
ROR1	98.33%	44.83%	53.50%
TGF-b RII	94.42%	39.02%	55.40%

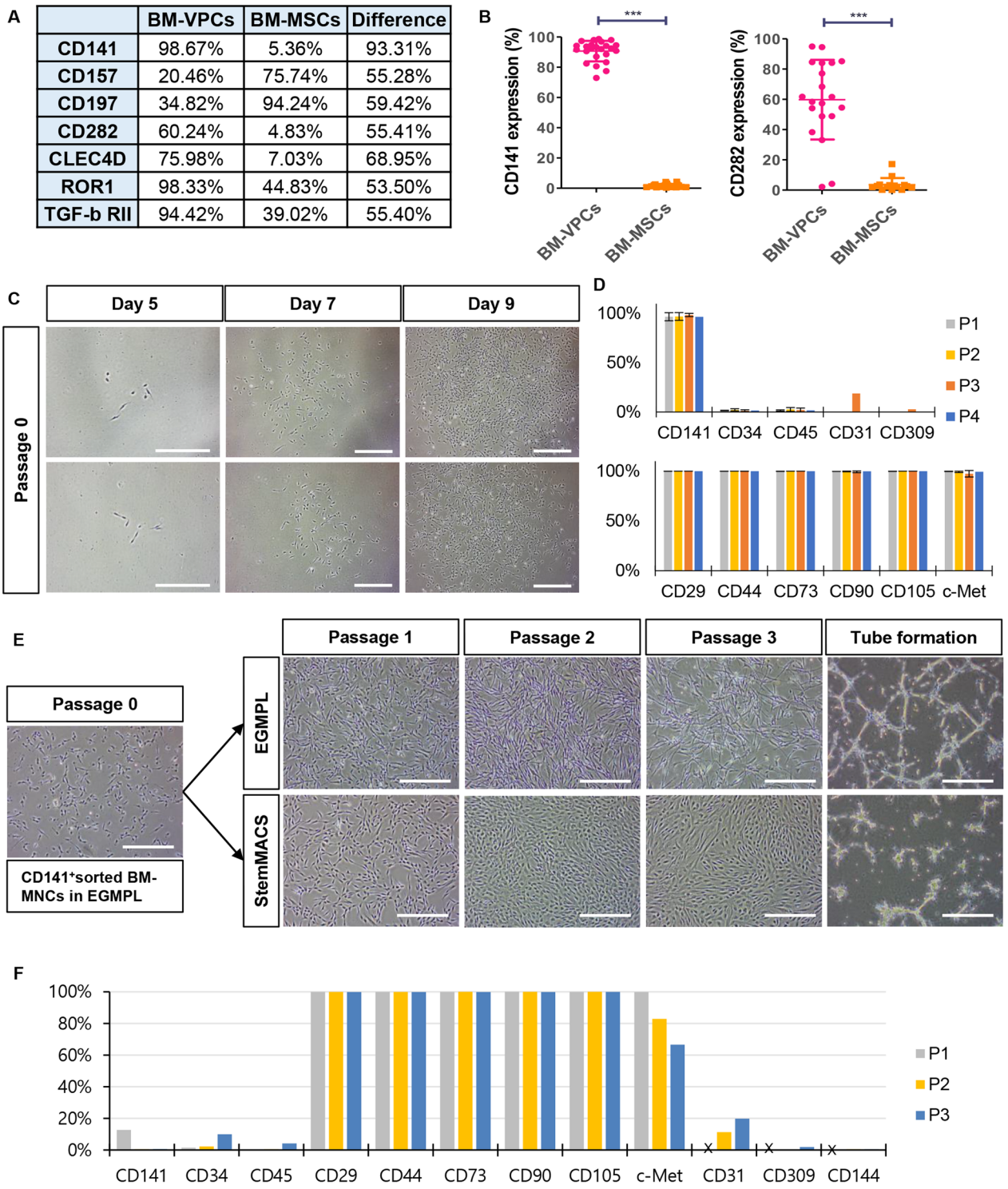

Fig. 3 CD141 is a critical marker that distinguishes BM-VPCs from BM-MSCs. **A** List of markers with an expression difference of > 50% between BM-VPCs and BM-MSCs screened among 376 surface markers. **B** Differential expression of CD141 and CD282 in 15–20 donors assessed using flow cytometry analysis (***$p < 0.001$, Student's t-test, two-tailed). **C–F** BM-MNCs were sorted using magnetic bead-conjugated CD141 antibody. The selected MNCs were plated in EGMPL. **C** Colonies that appeared from CD141$^+$ sorted BM-MNCs on days 5, 7, and 9. Scale bar = 500 μm. **D** Marker expression profile of ex vivo-cultured cells from CD141$^+$ sorted colonies at passages 1 to 4 analyzed using flow cytometry. **E, F** CD141$^+$ sorted BM-MNCs were cultured in EGMPL at passage 0; from passage 1 to 3 and then, the cells were divided and cultured in EGMPL or StemMACS. **E** Morphology of replated CD141$^+$ sorted cells in EGMPL and StemMACS at passages 1 to 3, and their tube-forming ability in MEMα + 0.2%hPL at passage 2. Scale bar = 500 μm. **F** Marker expression profile of CD141$^+$ sorted cells cultured in StemMACS

using magnetic cell separation and cultured in the EGMPL medium. Colonies emerged from CD141-sorted cells and expanded with PDT similar to that of unsorted BM-MNC cultures, up to passage 4 (Fig. 3C, Additional file 1: Table S4). In addition, their surface marker expression pattern—positive for CD141, CD29, CD44, CD73, CD90, CD105, and c-MET, and negative for CD31, CD34, CD45, and CD309—was identical to that of unsorted BM-MNC culture in the EGMPL medium (Fig. 3D). Thus, $CD141^+$BM-VPCs preexisted in the human BM and could be expanded under specific growth conditions provided by EGMPL used in this study. Unsorted BM-MNCs cultured in StemMACS lacked vasculogenic capacity (Fig. 2A) and CD141 expression (Fig. 3B, Additional file 1: Figure S8, S9). Similarly, the CD141-sorted cells at P0 in the EGMPL could not maintain their CD141 expression or vasculogenic capacity when the culture medium was switched to StemMACS from passage 1 (Fig. 3E, F, Additional file 1: Figure S10). Maintenance of the phenotype and expansion of preexisting CD141-expressing vasculogenic clones may require specific culture conditions, such as those provided by EGMPL.

$CD141^+$BM-VPCs possess multipotent differentiation capacity similarly to BM-MSCs

Expression of CD141 and other markers in BM-VPCs and BM-MSCs was confirmed using western blot analysis and immunofluorescence staining (Fig. 4A, B). CD141 was expressed in BM-VPCs but not in BM-MSCs. Alpha-smooth muscle actin (α-SMA), a marker for MSCs, pericytes, and myofibroblasts [29], was expressed in BM-MSCs but mostly not in BM-VPCs. Transgelin (TAGLN), a marker for smooth muscle cells [30] was expressed in both the cell types even though its expression was lower in BM-VPCs.

According to the definition of MSCs proposed by International Society for Cell and Gene Therapy (ISCT), MSCs adhere to plastic surfaces, are $CD105^+$, $CD73^+$, $CD90^+$, $CD34^-$, $CD45^-$, $CD14^-$, $CD11b^-$, $CD79^-$, $CD19^-$, and HLA-DR^-, and exhibit multipotent differentiation potential for adipocytes, osteocytes, and chondrocytes [31]. Because BM-VPCs matched several MSC criteria (Fig. 1F, Additional file 1: Figure S8, S11), we explored their multipotent differentiation capacity (Fig. 4C). Similar to BM-MSCs, BM-VPCs differentiated into adipocytes, osteocytes, and chondrocytes under appropriate conditions. Therefore, BM-VPCs are CD141-expressing immature cells that retain multipotency, but preferentially reveal their vasculogenic capacity.

HGF/c-MET signaling may play a role as an autocrine vasculogenic factor, especially in BM-VPCs

HGF is an angiogenic factor that stimulates EC motility and growth [32]. To investigate the potential involvement of HGF and c-MET in the autocrine vasculogenic capacity of BM-VPCs (Fig. 1D), the expression levels of HGF and c-MET in BM-VPCs were assessed (Fig. 4D, E). The expression of c-MET was much higher in BM-VPCs than in BM-MSC, and that of HGF in the culture supernatant was also higher in BM-VPCs, being 30–45 ng/ml in all passages of BM-VPCs, but was negligible in BM-MSCs. Furthermore, to explore autocrine vasculogenic contribution of BM-VPCs-secreted HGF, HGF levels were examined in the BM-VPCs culture in angiogenic factor-deficient MEMα + 0.2%hPL medium (Fig. 4F). BM-VPCs secreted HGF at ~ 10 ng/ml, which was approximately nine-fold higher than that secreted by BM-MSCs. Pretreatment with PHA-665752, a c-MET inhibitor, reduced vascular network formation in BM-VPCs (Fig. 4G, H). Thus, BM-VPCs highly express HGF and c-MET compared to BM-MSCs, which may help their vasculogenic capacity using HGF as an autocrine factor. Collectively, through extensive phenotypic characterization, BM-VPCs were identified as CD141-positive vasculogenic multipotent stem cells.

(See figure on next page.)

Fig. 4 Multipotency of BM-VPCs and angiogenic marker expression. **A** Comparison of the expression of CD141, α-SMA, and TAGLN in BM-VPCs and BM-MSCs using western blot analysis. GAPDH was used as a loading control. **B** Immunofluorescence images showing expression of CD141 and α-SMA in BM-VPCs and BM-MSCs. Green = CD141; Red = α-SMA; Blue = DAPI. Scale bar = 100 μm. **C** Images of Oil red O-, Alizarin red S-, and Alcian blue-stained differentiation-induced BM-VPCs and BM-MSCs. yellow scale bar = 50 μm, white scale bar = 200 μm, black scale bar = 300 μm. **D** Comparison of c-MET expression in BM-VPCs and BM-MSCs using western blot analysis. α-tubulin was used as a loading control. **E** HGF concentration at passages 1 to 3 in cell culture supernatants measured using ELISA (***p < 0.001, one way ANOVA test followed by Turkey's multiple comparison test, n = 4). **F** HGF secretion by BM-VPCs and BM-MSCs under growth factor-defective culture condition (MEMα + 0.2%hPL), assessed using ELISA. Values are mean ± SD (****p* < 0.001, Student's t-test, two-tailed, n = 3). **G** Images showing in vitro Matrigel tube-forming ability of BM-VPCs with or without PHA-665752 200 nM, a c-MET inhibitor. Scale bar = 500 μm. **H** Quantitative analysis of in vitro tube formation. Different parameters were measured using an angiogenesis analyzer in the Image J software. Values are mean ± SD (**p* < 0.05, ***p* < 0.01, ****p* < 0.001, student's t-test, n = 5)**.** Full-length blots are presented in Figure S17

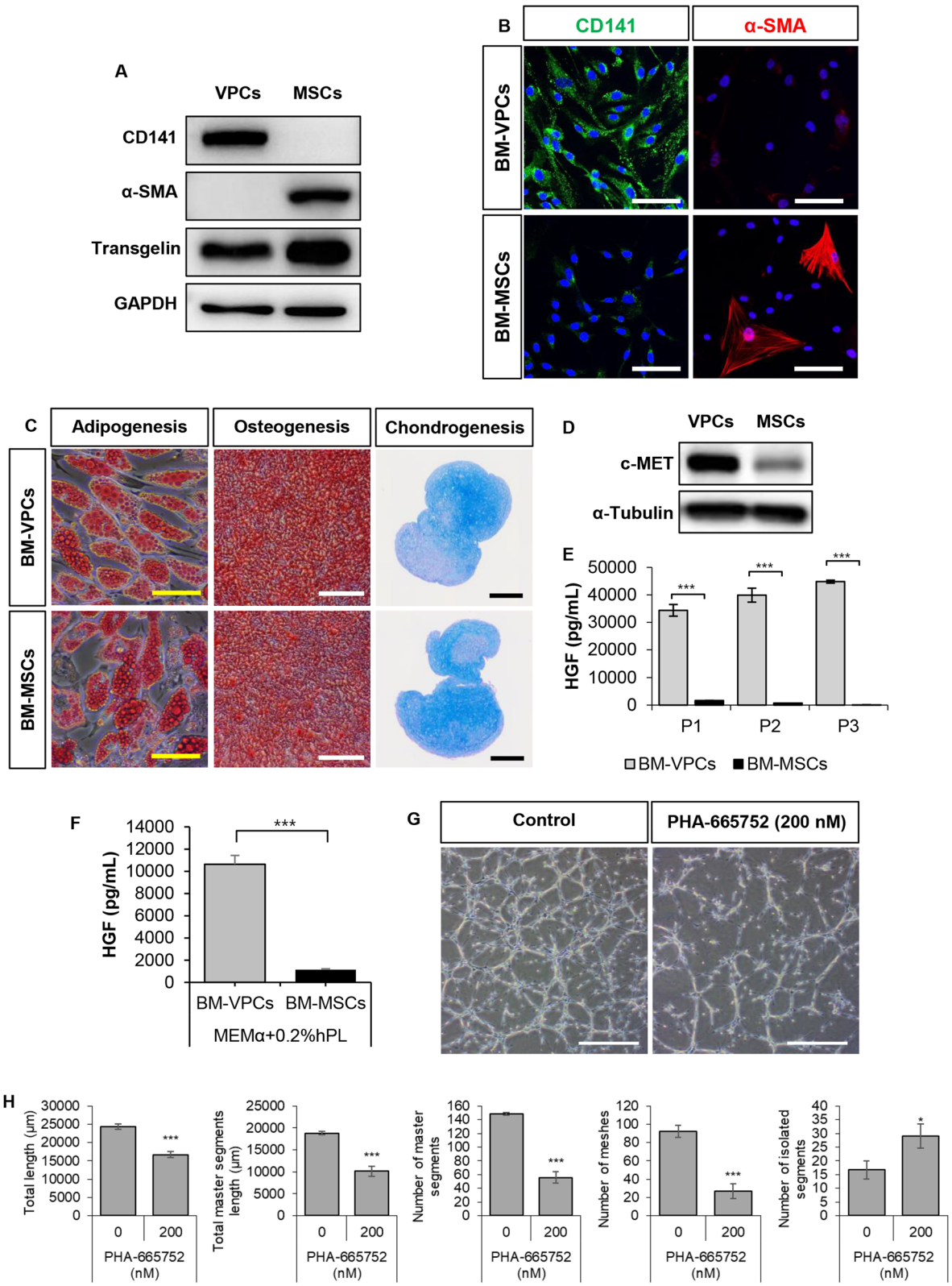

Fig. 4 (See legend on previous page.)

Transplantation of a combination of CD141$^+$ VPCs and BM-MSCs is more effective than transplanting them individually

To evaluate the efficacy on vascular repair, a nonclinical hindlimb ischemia model was established in nude mice using different surgical techniques (Additional file 1: Figure S12). Severe hind limb ischemia, which substantially reduced the blood flow up to 20% of that in the contralateral normal side, was chosen to assess the extent of restoration achievable with cell therapy. The severity of limb damage was standardized by scoring gross views of the mouse limbs, feet, and toes and classified into seven stages—grade 0 for limb salvage and grade 6 for limb loss (Additional file 1: Figure S3).

The efficacy of transplantation of CD141$^+$VPCs or BM-MSCs and their combination was compared using the CLI model by intramuscularly injecting 1.2×10^5 cells/50 µL of a 2:1 mixture of human BM-derived CD141$^+$ VPCs and BM-MSCs at passage 3 or the same number of either cell type at five different sites along the artery-excised area (Fig. 5A, Additional file 1: Figure S2). As evident from gross views of the limb at 4 weeks, only the dual cell group could consistently rescue the limb or part of it, whereas the limb was lost within 7 days in the saline-injected group (Fig. 5B–D). Furthermore, transplantation of either CD141$^+$ VPCs or BM-MSCs could not salvage the limb, and toe or foot was lost. The effect of cell transplantation was evident on day 1 and almost plateaued on day 7. A clear difference was noted between dual cell and singular transplantation as early as on day 2, which almost plateaued at day 3, resulting in limb salvage at day 7, which was sustained for up to 4 weeks. In contrast, the BM-MSC-only group showed a higher ischemic score than the CD141$^+$VPC-only group over 4 weeks (Fig. 5C). At 4 weeks, the dual cell and CD141$^+$VPC-only groups rescued the limb in ~ 90% and ~ 20%, but BM-MSC-only group could not (Fig. 5D). On day 7, the blood flow in the ischemic limb in the dual cell group, measured using a laser Doppler blood flow imager, was recovered to ~ 80% of that in the contralateral normal side and continuously increased to 100% at 4 weeks (Fig. 5E, F). In addition, the group that received singular transplantation showed lower recovery compared to the group that received the dual cell transplantation. The CD141$^+$VPCs-only group showed better recovery than the BM-MSCs-only group, for which recovery was not sustained at later stages. According to the ischemic score and blood flow recovery, the combination of CD141$^+$VPCs and BM-MSCs was the most effective, and the CD141$^+$VPCs-only group was more effective than the BM-MSCs-only group.

The transplanted cells may be involved in vessel regeneration at the ischemic site for blood flow recovery and limb salvage. Cross sections of dual cell-transplanted ischemic limb were stained with human CD31-specific antibodies for ECs and human α-SMA-specific antibodies for smooth muscle cells and pericytes (Fig. 5G–J, Additional file 1: Figure S13). Dual cell-transplanted mice exhibited large CD31$^+$/ α-SMA$^+$ vasculature. In contrast, CD141$^+$VPCs-transplanted mice displayed only a few CD31$^+$ but α-SMA$^-$ vessel, whereas BM-MSCs-transplanted mice showed a few α-SMA$^+$ but CD31$^-$ vessels (Fig. 5I, J).

Dose response of dual cells on vascular repair

To determine the optimal cell number for vascular repair and blood flow recovery, we injected three different doses of 2:1 combination of CD141$^+$ VPCs and BM-MSCs: low (1.2×10^4 cells/50 µL), mid (1.2×10^5 cells/50 µL), and high (1.2×10^6 cells/50 µL) to each mouse (Fig. 6). Based on the ischemic score and blood flow recovery over 4 weeks, the mid dose was the most and the low dose was the least effective; the high dose was effective in limb salvage but was apparently excessive (Fig. 6A–C).

In immunofluorescence staining, large vessels encircled by a thick TAGLN$^+$ smooth muscle layer were frequently detected at the injury site in the mid- and high-dose injection groups (Fig. 6D–G). Thus, 1.2×10^5 cells/50 µL was considered to be the optimal dose for this CLI model.

Dual cell transplantation led to the formation of arteries and arteriole-like vessels at the injury site on day 7, which increased in diameter at 4 and 12 weeks

Based on the ischemic necrosis score (Additional file 1: Figure S3), the therapeutic effect of dual cell

(See figure on next page.)

Fig. 5 Limb salvage in hind limb ischemia requires a combination of CD141$^+$ VPCs and BM-MSCs. **A** To compare the efficacy of dual stem cell therapy with singular cell type therapy, CD141$^+$VPCs, BM-MSCs and their combination were administered in a CLI model. **B** Changes in the limb over a 4-week period. Dotted circle: CLI-induced site. **C** Ischemic necrosis grade over the 4-week period; 2-Way ANOVA test with Tukey multiple comparisons. **D** Distribution of grades for ischemic necrosis across all groups at 4 weeks post-surgery. **E** Images of laser Doppler measurements over 4 weeks was acquired and **F** blood flow was relatively quantified; 2-Way ANOVA test with Tukey multiple comparisons **G, H** Immunofluorescence images for human CD31 **G** and human a-SMA expression **H** at 4 weeks **I, J** Qualification of human CD31 **(I)** and human a-SMA **(J)**; Kruskal–Wallis test with Tukey multiple comparisons. $N = 8$/group. Scale bar = 100 µm. p values < 0.05 were considered statistically significant. ***$p < 0.001$ dual cells vs. saline; ++$p < 0.01$, +++$p < 0.001$, dual cells vs. CD141$^+$VPC; #$p < 0.05$, ##$p < 0.01$, ###p < 0.001 dual cells vs. BM-MSCs; $p < 0.05, $$p < 0.01, $$$p < 0.001 saline vs. CD141 + VPCs; &&p < 0.01, CD141 + VPCs vs. BM-MSCs

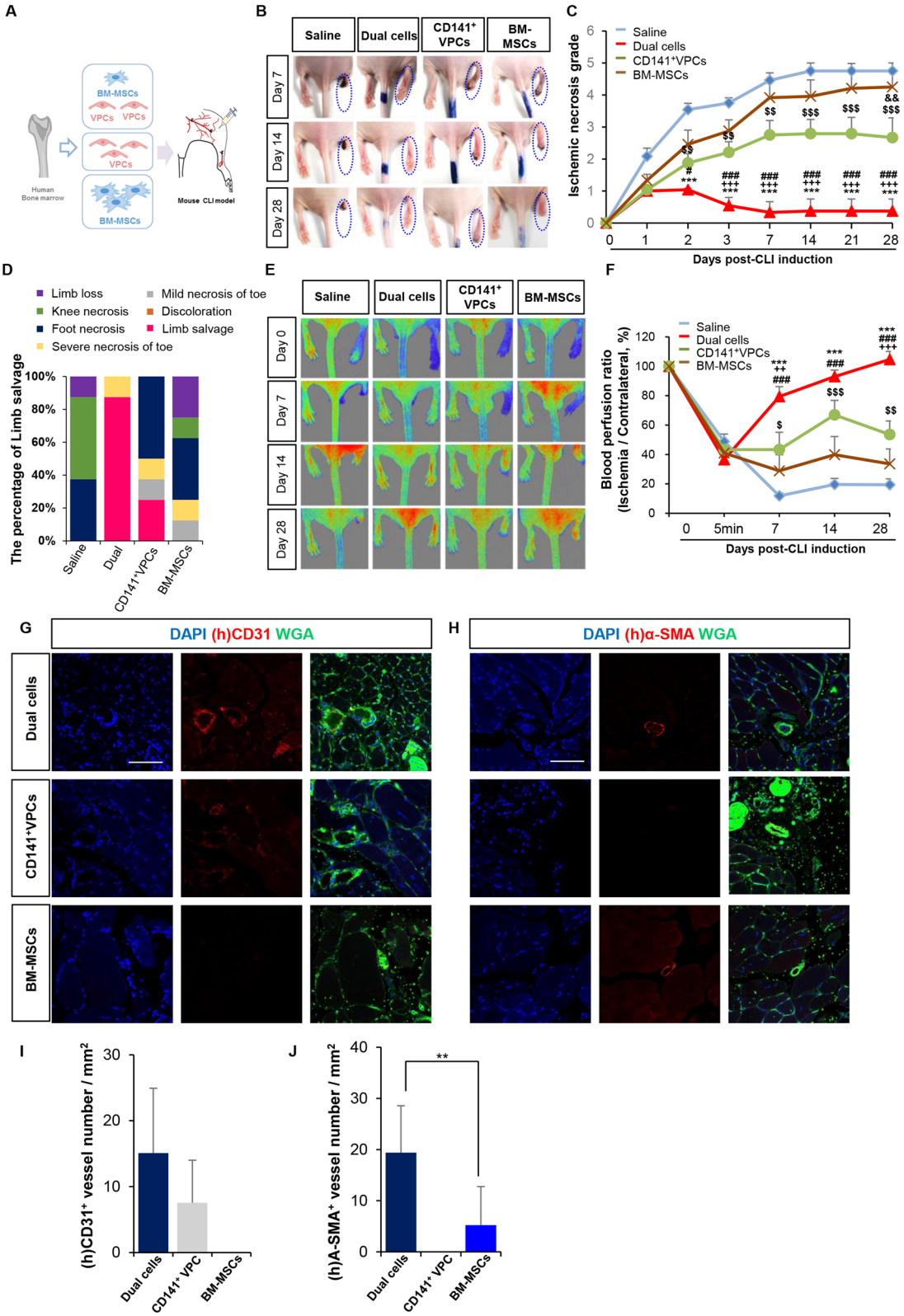

Fig. 5 (See legend on previous page.)

transplantation became obvious on day 3, and blood flow recovery was apparent on day 7 (Figs. 5F, 6C), indicating rapid manifestation of beneficial effects. The effect of dual cell transplantation on vascular repair was explored in the early phase (Fig. 7A–G). The difference in ischemic scores between the dual cell and saline groups was evident on day 2, and limb necrosis was evident on day 3 in the saline group (Fig. 7A). In the dual cell transplantation group, blood flow recovery was obvious on day 3, reaching approximately 80% on day 7; however, blood flow insufficiency was obvious on day 3 in the saline group (Fig. 7B). Macroscopic examination of the injured limb on day 7 revealed restoration of a large vessel (white arrowhead) within the muscle, where the superficial femoral artery was removed (white dotted line), in the dual cell group. In contrast, in the saline group, the muscle displayed severe inflammation (black star) and did not show neovascularization (Fig. 7C).

Arteries and arterioles, characterized by their large size and sufficient coverage of the vascular smooth muscle cell (VSMC) media layer, were detected at the injury site by immunofluorescence staining of TAGLN, a representative VSMC marker, and Alexa 488-labeled wheat germ agglutinin (WGA) for muscle and vessels (Fig. 7D, E). The dual cell group showed numerous TAGLN$^+$ vessels on day 3, which became larger on day 7, whereas the saline group displayed fewer and smaller TAGLN$^+$ vessels. Quantitative analysis of vessel density and diameter further confirmed that dual cell transplantation increased the vessel density and the number of vessels with diameters larger than 20 μm was approximately 2.7-fold more than in the saline group on day 7 (Fig. 7F, G). In mice, vessel with diameters > 20 μm are classified as arterioles [33].

At 4 weeks, a new large vessel restored at the injury site, where numerous arteries and arterioles bifurcated from the main artery, was clearly observed in the dual cell group (Fig. 7H). Severe inflammation and fibrosis were evident in the remaining tissues in the saline group. After tissue clearing, the 3-D architecture of CD31$^+$ vessels was observed using whole-mount analysis (Fig. 7I, J). Normal limb showed a large CD31$^+$ femoral artery with mean diameter of 321.7 ± 21.9 μm. In the dual cell group, abundant CD31$^+$ vessels were detected, corresponding to approximately 90% of the vessel density in normal limb and mean diameter of 88.1 ± 5.5 μm in the large vessel. However, in the saline-treated group, thin CD31$^+$ vessels were scarcely detected, and CD31$^+$ vessel density was approximately 20% of that in the normal limb.

The characteristics of the restored vessels at 4 weeks were analyzed using immunofluorescence staining with TAGLN and WGA, followed by quantitative analysis of vessel density and size (Fig. 7K–N). The dual cell group displayed numerous vessels with a larger diameter and a thicker TAGLN$^+$ VSMC media layer than the saline group. Quantification of TAGLN$^+$ vasculature showed that the dual cell group exhibited a varied range of vessel diameters, including 28% of TANGL$^+$ vessels with a diameter > 20 μm (Fig. 7N; < 20 μm: 72%; 20–50 μm: 25%; > 50 μm: 3%; average: 17.71 μm) but the saline group showed small vessels with a diameter mostly < 20 μm.

In addition, immunofluorescence staining at 12 weeks revealed numerous large-diameter vessels uniformly covered by the TAGLN$^+$ thick VSMC media layer in the dual cell group (Fig. 7O). The vessel density in the dual cell group was more than that in the saline group and the mean diameter was ~ 37 μm, which was larger than that at 4 weeks. Vessels with diameter > 50 μm were ~ 13%, most clearly detected in the dual cell group (Fig. 7P–R). The effects of the dual cell transplantation on blood flow recovery and limb salvage were maintained for up to 24 weeks (Additional file 1: Figure S14).

Dual cells were engrafted in the restored large vessel as human CD31$^+$ intima and human α-SMA$^+$ VSMC layer at 4 and 12 weeks

The fate of transplanted human CD141$^+$VPCs and BM-MSCs in restored vessels was confirmed using immunofluorescence staining with human CD31 and human α-SMA-specific antibodies and WGA staining for vascular and muscle histology (Fig. 8A). CD141$^+$VPCs were anticipated to function as the vessel endothelium and BM-MSCs to cover vessels as the vascular smooth muscle of arteries or arterioles. The human CD31$^+$ inner lining and human α-SMA$^+$ media layer of vessels, both of which are stained with

(See figure on next page.)

Fig. 6 Optimization of dose for dual cell transplantation in CLI model. Dual cells were transplanted into CLI mice model at three different doses (High: 1.2×10^6; Mid: 1.2×10^5; Low: 1.2×10^4). **A** Assessment of ischemic necrosis grade over 4 weeks; 2-Way ANOVA test with Tukey multiple comparisons. **B** Distribution of grades for ischemic necrosis across all groups at 4 weeks post-surgery. **C** Images of laser Doppler measurements over 4 weeks together with relative quantification data; 2-Way ANOVA test with Tukey multiple comparisons. **D** Immunofluorescence images for human/mouse CD31 expression. WGA was used to label the muscle structure. **E** Immunofluorescence images for TAGLN. DAPI was used for counterstaining and WGA was used to label the muscle structure. **F, G** The quantification of human/mouse CD31 and TAGLN vessel number (Kruskal–Wallis test with Dunn's multiple comparisons). N = 8/group. Scale bar: 100 μm. ##$p < 0.01$, ###$p < 0.001$ High dose vs. Saline; + p < 0.05, High dose vs. Low dose; *$p < 0.05$, ***$p < 0.001$ Mid dose vs. Saline; $$p < 0.05$, $$$p < 0.01$, $$$$p < 0.001$ Mid dose vs. Low dose

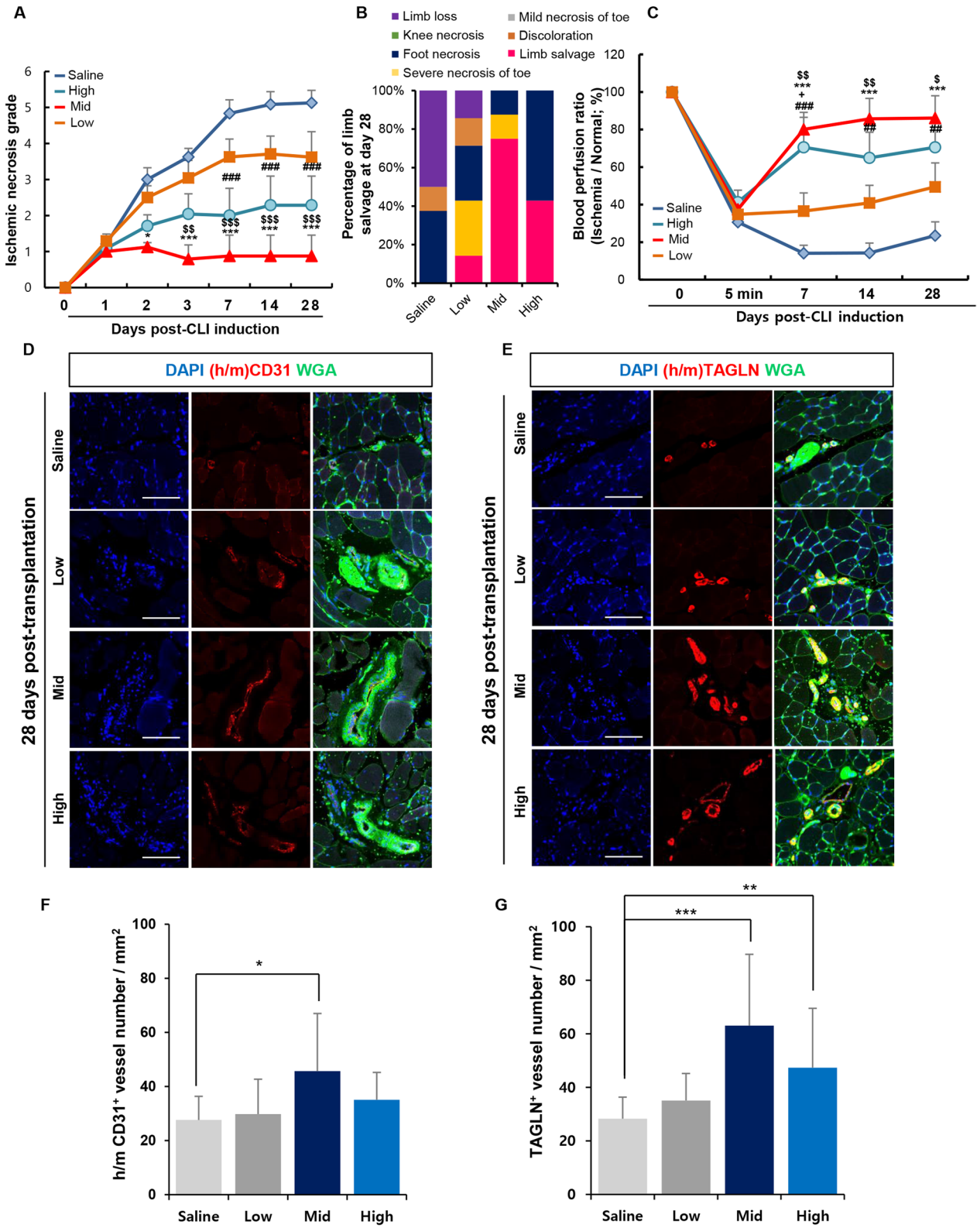

Fig. 6 (See legend on previous page.)

WGA, were detected in the muscle at the injury site in the dual cell group at 4 weeks (Fig. 8A). Double immunofluorescence staining with human/mouse reactive α-SMA and human-specific CD31 antibodies showed a human $CD31^+$ inner lining of the large vessel, tightly encircled by a thick α-SMA-covered smooth muscle layer (Fig. 8B). Among the vessels at the injury site, the endothelial lining engrafted by transplanted human cells was distinguished from that of mouse vessels using double immunofluorescence staining with human CD31 and human/mouse-reactive CD31 antibodies (Fig. 8C). The human cell-engrafted vasculature was identified by human $CD31^+$ and human/mouse $CD31^+$ vessels (white arrowheads), which were mostly larger than human $CD31^-$ and human/mouse $CD31^+$ vessels, presumably mouse vessels (yellow arrowheads). Human $CD31^+$ vessels were frequently detected among large-diameter vessels, possibly contributed by human $CD141^+$VPCs in the transplanted dual cells. At 12 weeks, human α-SMA^+ large vessel, which was also stained with $TAGLN^+$ media layer, was detected in serially sectioned muscle samples (white asterisk), indicating the long-term vascular integration of transplanted human cells, possibly BM-MSCs (Fig. 8D). Notably, human α-SMA^+/$TAGLN^+$ vessels appeared larger in diameter than human α-SMA^-/$TAGLN^+$ vessels in the next section, presumably mouse vessel (yellow arrows). Immunofluorescence staining of serially sectioned samples with human α-SMA and human/mouse calponin antibodies along with WGA showed that human cell-engrafted large vessel was positive for human α-SMA and calponin staining at 12 weeks (Additional file 1: Figure S15). Collectively, transplanted human $CD141^+$VPCs and BM-MSCs functioned as reparative cells in the restored vessels at the injury site up to 12 weeks after transplantation, and were probably fated to human CD31-expressing ECs and human α-SMA-expressing smooth muscle cells, respectively.

Transplanted human dual cells were detected only in injected muscle even at 16 weeks post transplantation

To further analyze the distribution of the transplanted dual cells, $CD141^+$ VPCs and BM-MSCs were labeled with DiR before transplantation, and the fluorescence intensity was monitored until 16 weeks using an in vivo imaging system (Fig. 8E, F). Fluorescence intensity decayed exponentially up to 16 weeks (D112) but was detectable at the injection site at 16 weeks. In the organ biopsy at 16 weeks, DiR fluorescence was detected only in the injected muscle and not in other organs (Fig. 8G). In addition, DiR fluorescence was observed in vessel-like structures in the muscle (Fig. 8H). Furthermore, human $CD31^+$ and α-SMA^+ staining was visible in the inner lining of the vessel and media layer of the WGA^+ vessels, respectively, which may indicate vascular integration of transplanted cells during vascular remodeling under homeostatic turnover (Fig. 8I). In addition, human CD31 was detected by immunohistochemical staining (Fig. 8J). Again, by western blot analysis, human CD31 protein (82 kD) was clearly detected in the injected muscles of the CLI mouse at 2 weeks post-transplantation and also in the normal mouse at 16 weeks post-transplantation, supporting the in vivo endothelial differentiation of dual cells, possibly $CD141^+$VPCs (Fig. 8K). The RT-PCR analysis of human ALU DNA (FAM) over 26 weeks also revealed the presence of human cells in the injected calf muscle (Additional file 1: Table S5, 6).

Discussion

In this study, a novel, multipotent VPCs with neovascularization capacity was identified in human BMA. These VPCs were distinct from previously reported EPCs by the lack of several endothelial surface markers, such as VE-cadherin, CD31, VEGFR2, and CD34, and their high in vitro cell expansion capacity. Through surface marker screening, these VPCs were found to express CD141, thrombomodulin, and several other surface markers that were distinguishable from BM-MSCs

(See figure on next page.)

Fig. 7 Dual cells induced the formation of arteriole-like vasculature at injury site within 7 days of transplantation. **A** Scoring of ischemic necrosis. $^{**}p < 0.01$ and $^{***}p < 0.001$ vs. saline-treated group (Student's t-test, two-tailed). **B** Quantification of blood restoration. $^{***}p < 0.001$ vs. saline-treated group (Student's t-test, two-tailed). **C** Injury site at day 7 (White dotted line: excised femoral artery; white arrowhead: new vessels; yellow arrowhead: femoral nerve; black star: purulent; 1–3: ligated site). **D, E** Immunofluorescence images for human/mouse TAGLN; DAPI was used for counterstaining and WGA was used to label muscle structure. Scale bar = 100 μm. **F, G** Quantification of $TAGLN^+$ vasculature. **H** Comparison of the vasculature in the ischemic zone at 4 weeks post-dual cell transplantation (white arrowhead: new vessels; yellow dotted lines: excision of the femoral artery; yellow arrowhead: femoral neuron). **I, J** Whole-mount images of $CD31^+$ vessels at injury site and their quantitative analysis. Scale bar = 200 μm. **K–N** Immunofluorescence images for human/mouse $TAGLN^+$ vessels and their density and diameter at 4 weeks post-transplantation. Scale bar = 100 μm. **O–R** Immunofluorescence images for human/mouse $TAGLN^+$ vessels and their density and diameter at 12 weeks post-transplantation. Scale bar = 100 μm. $N = 8$/group. $p < 0.05$ indicates statistical significance. $^{*}p < 0.05$, $^{**}p < 0.01$ and $^{***}p < 0.001$ vs. saline-treated group (Student's t-test, two-tailed). WGA: Wheat germ agglutinin

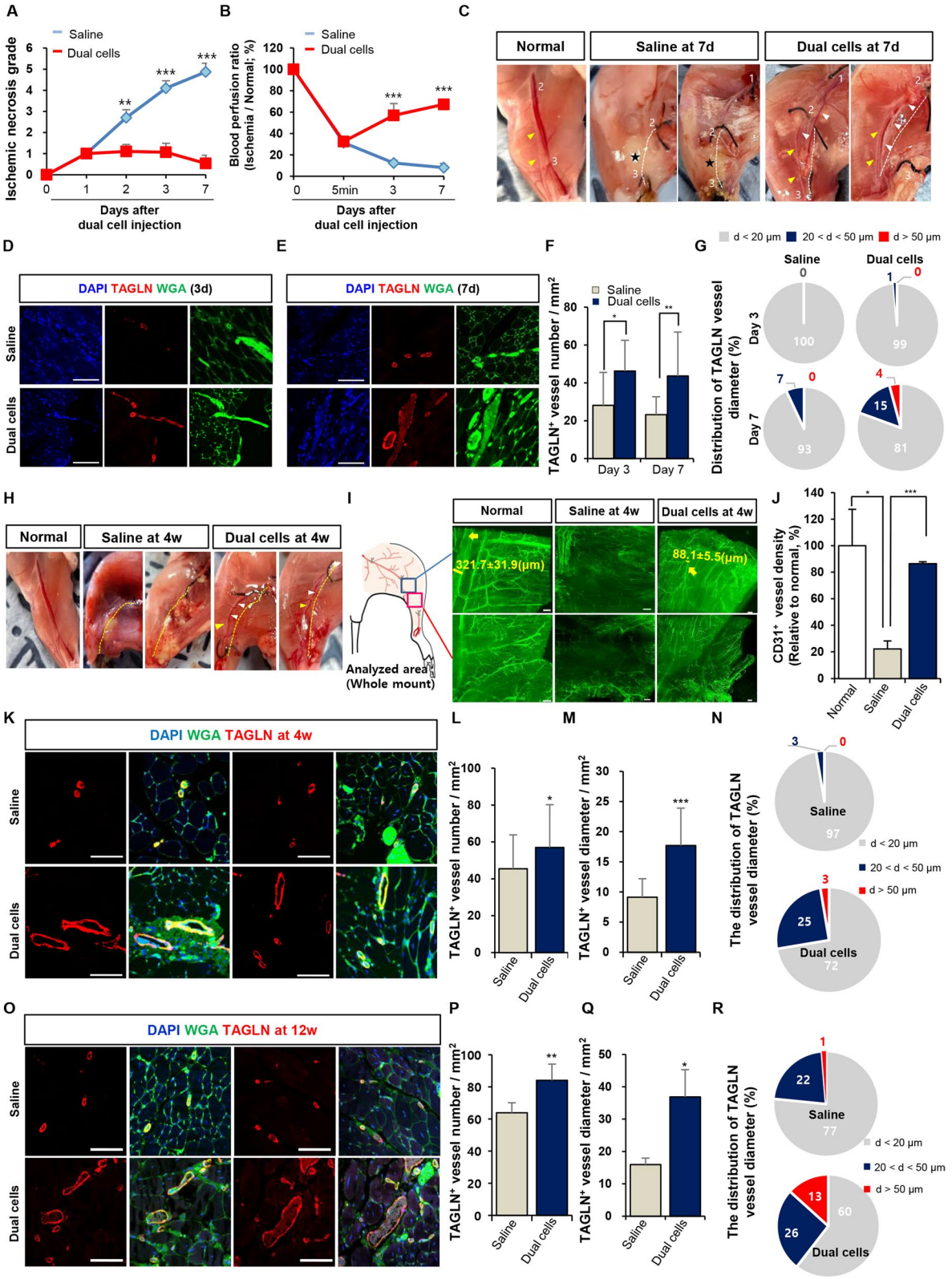

Fig. 7 (See legend on previous page.)

in the BMA. Moreover, CD141-sorted cells from whole MNCs of BMA generated VPC colonies, with the same cellular phenotype as that of the CD141-unsorted culture. Importantly, VPCs recruited non-vasculogenic BM-MSCs to the branching points and segments of the vascular network like tightly encircling pericytes in a 2:1 combination of VPCs and BM-MCs. Additionally, the VPCs generated a combined vascular network with HUVECs in vitro, supporting angiocrine effect of VPC-secreted HGF. In an efficacy test using a severe CLI model in nude mice, dual cell transplantation at the optimal dose preserved the limb, restored a large artery at the excised injury site, and normalized blood flow within 4 weeks. This approach was superior to the singular transplantation of VPCs or BM-MSC. Furthermore, human CD31-expressing endothelial intima and human α-SMA-expressing VSMC media layers were frequently detected in the restored large arteries in the dual cell transplantation group up to 12 weeks. In contrast, only human CD31-expressing intima in the VPCs and only human α-SMA-expressing VSMC media layer in the BM-MSC transplantation groups were scarcely detected, suggesting that CD141 + VPCs may give rise to ECs, while BM-MSCs may differentiate into vascular smooth muscle cells in vivo. The novel $CD141^{+}$VPCs in combination with BM-MSCs can be further developed as a vascular replacement therapy to treat PAD or other ischemic vascular diseases.

$CD141^{+}$VPCs identified in this study were a highly clonogenic and multipotential subset of BM-MNCs, residing in the BM as a rare population that were specifically expanded under the hPL-supplemented endothelial selective culture medium, with mean PDT of ~ 20 h up to passage 3, yielding ~ 2×10^{10} VPCs within 3 weeks starting with 1×10^{7} BM-MNCs corresponding to 0.2–10 ml BMA depending on the donor (Additional file 1: Table S2, 3). This cell expansion capacity enables the development of autologous vasculogenic cell therapies. Optimal cell dose for the best efficacy in CLI model was 1.2×10^{5} cells in a 2:1 combination of VPCs and BM-MSCs, which can be extrapolated to 3×10^{7} cells/60 kg human equivalent dose based on body surface area (human equivalent dose; HED) [34] or a maximum of 3×10^{8} cells/60 kg based on previous clinical trials of MSCs derived from a variety of sources [35], which can be fully covered by the cell expansion capacity of VPCs from human BMA. Moreover, no tumors were formed for 26 weeks, even when 83 times more cells than the optimal effective dose were administered (Additional file 1: Table S7). However, the effective nontoxic dose and optimal cell delivery should be further investigated in clinical studies. This study provides a stepping stone for clinical trials on severe PAD, especially in Rutherford class 4–5, which may ultimately lead to amputation of the lower extremities if not treated effectively [36]. In particular, the better efficacy of dual cell transplantation provides a rationale for combinatorial cell therapy for a variety of tissue repair.

CD141, a thrombomodulin, is primarily localized in vascular ECs and many other cells, such as monocytes, dendritic cells, and limbal stem cells [37], and is expected to integrate a variety of biological processes, such as anticoagulation, inflammation, innate immunity, tissue regeneration, and angiogenesis to protect the host from injury and promote healing [26]. Previous report strongly supports the role of CD141 in the podosome assembly of tip cells during sprouting angiogenesis [27]. Based on this study, CD141 in BM-VPCs seems to be important for the expression of its vasculogenic phenotype, which can be affected by several factors during culture [38]. CD141 is a unique marker for distinguishing vasculogenic BM-VPCs from non-vasculogenic BM-MSCs, even though both cell types share many cellular characteristics. $CD141^{+}$VPCs at P0 rapidly lost their CD141 expression and vasculogenic capacity by switching VPCs-selective culture conditions

(See figure on next page.)

Fig. 8 Dual cells enhance vascularization by integrating into host vasculature. **A** Immunofluorescence images for human CD31 and human α-SMA showing the presence of transplanted cells. Scale bar = 100 μm. **B** Immunofluorescence images for human CD31 and human/mouse α-SMA showing human antigen-positive vessels with smooth muscle cells. Blue box: enlarged images. Scale bar = 100 μm. **C** Immunofluorescence images for human CD31 and human/mouse CD31 distinguishing human cell-integrated vessel from the host vessel (white arrowhead: human $CD31^{+}$ vessel; yellow arrowhead: host vessel) Scale bar = 100 μm. **D** Serially sectioned samples stained for human α-SMA and human/mouse TAGLN to identify vessels incorporating human cells. White asterisk: vessels double-positive for human α-SMA and human/mouse TAGLN, yellow arrows: vessels negative for human α-SMA and positive for human/mouse TAGLN. WGA was used to label muscle structure. Scale bar = 100 μm. **E, F** Distribution of DiR-labeled transplanted dual cells assessed using in vivo imaging under non-injured condition, with fluorescence intensity quantified up to 112 days post-transplantation. **G** Comparisons of the intensity among different organs. **H** DiR^{+} human cells at the muscle site. Scale bar = 100 μm. **I** Immunofluorescence images for human α-SMA and human CD31 showing transplanted human cells. Scale bar = 100 μm. **J** Immunohistochemical images for human CD31in muscle sections of mouse subjected to dual cell transplantation. **K** Western blot analysis of human CD31 in the muscle of dual cell transplantation. At 2 weeks post-transplantation in CLI mice and at 16 weeks post-transplantation in normal mice, muscle tissue was lysed to extract total protein, which was then analyzed for human CD31 expression by western blotting. Human aortic endothelial cells (HAEC) were used as a positive control of human CD31 protein and muscle tissue from saline injected mice or the contralateral site of CLI mice were used as negative control of human CD31. Full-length blots are presented in S17. *N* = 8/group

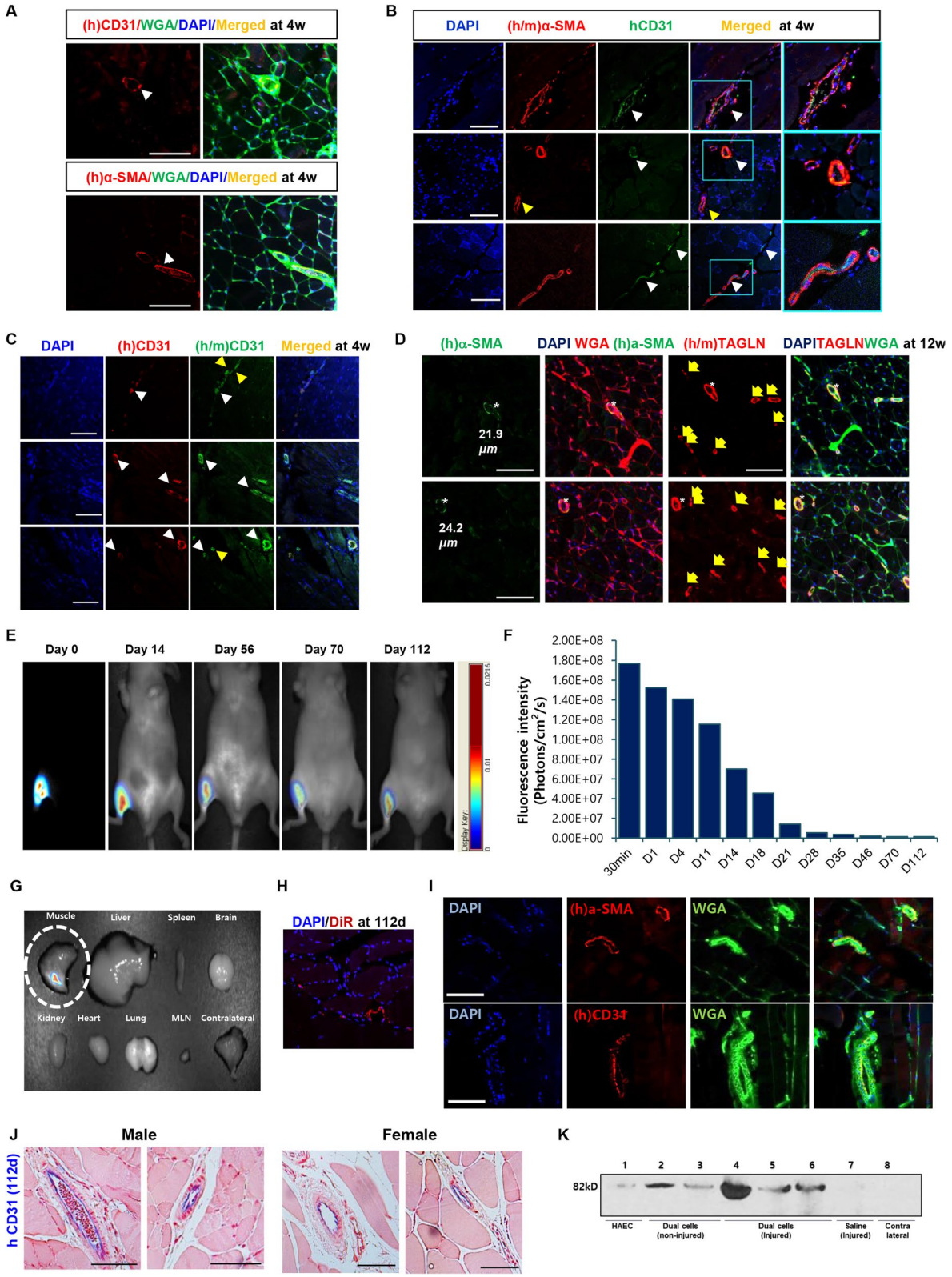

Fig. 8 (See legend on previous page.)

to BM-MSCs-selective culture medium (Fig. 3), which did not support the VPCs colonies from the same MNCs derived from BMA. However, a more definitive role for CD141 in the vasculogenic capacity of VPCs or the non-vasculogenic capacity of BM-MSCs needs to be explored by its overexpression or functional downregulation. Moreover, whether any specific factors included in the VPCs-selective culture medium, namely EGMPL, are more important for maintaining or regulating CD141 expression in VPCs needs to be explored. Nevertheless, the unique expression of CD141 in VPCs culture provides a marker to distinguish VPCs from BM-MSCs for quality control and assurance.

$CD141^+$ VPCs identified in human BMA were characteristically more similar to VPCs found during development [39] or induced from iPSCs [16], including iPSC-induced CD34 + progenitor cells [17], and VPCs genetically induced using Etv2 and Fli1 [19], than to tissue-resident VESCs expressing endothelial lineage markers such as VE-cadherin and CD31 [40]. These iPSC-induced VPCs or VPC-like cells could adopt both cell phenotypes under specific culture conditions: high VEGF for the endothelial phenotype and high PDGF-BB for the pericyte and VSMC phenotypes [16]. Accordingly, these VPCs may retain their bipotent differentiation capacity. In contrast, our $CD141^+$VPCs did not express most surface markers of definitive ECs, also revealed multipotent differentiation capacity similar to that of BM-MSCs, and lost their CD141 expression and vasculogenic phenotype in a context-dependent manner. Thus, $CD141^+$ VPCs may be a rare subpopulation of BM-MSCs or similar precursor cells stored in the BM.

Although human CD31 protein (82 kDa) was detected in the dual cell-injected muscle of both CLI model and normal mice via Western blot analysis (Fig. 8K), and human CD31 expression was observed in the intima of the restored vessel through immunofluorescence staining (Figs. 7, 8), this does not definitively prove that the CD31-expressing cells originated from $CD141^+$ VPCs in dual cell transplantation, rather than from BM-MSCs. In hybrid tube formation assays with HUVECs under proangiogenic conditions, or with BM-MSCs supplemented with TNF-α, $CD141^+$ VPCs enhanced CD31 expression during tube formation when co-cultured with BM-MSCs, TNF-α, and endothelial cells. This reflects the conditions that dual cell populations may encounter at the transplantation site. In contrast, BM-MSCs alone could not stimulate CD31 expression in the same environment. Moreover, in the muscle following the singular transplantation of BM-MSCs, only human α-SMA expression was detected, while no human CD31 expression was observed. Accordingly, it can be reasonably speculated that $CD141^+$ VPCs may differentiate into endothelial cells in an in vivo injured and inflamed environment when administered together with BM-MSCs, possibly aided by nearby endogenous endothelial cells. This differentiation could facilitate their involvement in arteriogenesis and angiogenesis, supported by the co-injected BM-MSCs. However, definitive evidence for the lineage differentiation of VPCs into endothelial cells and BM-MSCs into smooth muscle cells requires further investigation through individual cell tracing studies in vivo.

In dual cell transplantation, VPCs and BM-MSCs may cooperate to confer better survival and tissue engraftment in an inflammatory injury environment (Fig. 5); much less efficacy and lower engraftment was observed in VPCs or BM-MSCs transplantation than in a combination of both at the same cell number. Moreover, the human $CD31^+$ endothelial intima and human $\alpha\text{-SMA}^+$ smooth muscle media layer of the large vessel was frequently found for longer time in dual cell therapy. Our in vitro data that the vascular network of dual cells was well-sustained under TNF-α-supplemented environment unlike its partial disruption in VPCs-only transplantation supports this hypothesis. Importantly, various paracrine factors secreted by VPCs and BM-MSCs may also cooperate with each other for their survival and stimulation.

Functional blocking of HGF can inhibit VPC-stimulated sprouting of HUVECs in an indirect co-culture of VPCs and HUVEC spheroids [41]. We found secretion of HGF by VPCs (Fig. 4E). BM-MSC-secreted VEGF and several angiogenesis-related cytokines were also measured (Additional file 1: Figure S16). These molecules may cooperatively exert an angiogenic role in injured tissue in a paracrine manner. Anti-inflammatory effect of BM-MSCs is well recognized [42], which definitively confers an advantage for the survival of dual cells under the inflammatory environment. Collectively, VPCs and BM-MSCs share several paracrine factors and cellular contacts that regulate the inflammatory environment and stimulate vasculogenesis.

Our study has selected CLI model using young, healthy nude mice to evaluate the long-term efficacy of human cells without the influence of immunosuppressants, which could potentially affect stem cell activity and tissue repair. However, this model is limited in its ability to reflect the diverse pathological conditions associated with PAD. Especially, anti-angiogenic elevation such as thrombospondin-1 (TSP-1), which is known to be more important in the disease progression of PAD patients than proangiogenic change [43, 44], could not be considered in this study. TSP-1 binds surface CD47 of EPC and inhibits its angiogenesis through eNOS and VEGFR2 pathway[45]. $CD141^+$ VPCs express CD47 (99.97%) but exhibit minimal expression of eNOS and VEGFR2 (Fig. 1F, Additional file: Figure S4E, Figure S7),

distinguishing them from endothelial cells and endothelial progenitor cells (EPCs). This suggests that they may engage in an alternative TSP-1/CD47 pathway, potentially impacting their vasculogenic capacity, such as through the inhibition of FGF-2 [46]. Those possible implications of anti-angiogenic regulation in PAD patients should be considered in the future clinical study.

Arteriogenesis, characterized by the growth or bridging of existing collateral arterioles, can replace occluded vessels that are unable to provide adequate perfusion to a tissue and can compensate for the loss of function in occluded arteries [47]. The severe CLI model used in this study requires immediate restoration of functional arteries for limb salvage, which may be solely dependent on the arteriogenesis of preexisting collaterals and/or vasculogenesis in situ through the concerted action of transplanted dual cells via their direct vascular incorporation and indirect paracrine effect. In this study, the extent to which these two events contributed to the efficacy could not be resolved. However, the direct involvement of dual cell transplantation in artery restoration is obvious because human $CD31^+$ endothelial inner lining and human α-SMA^+ media layer were readily found in the large arteries up to 12 weeks, but small vessels mostly representing capillaries and arterioles were all of murine origin. This suggests that transplanted human cells may be preferentially engaged in the regeneration of arteries and arterioles, which may be further remodeled into larger vessels rather than capillaries. Notably, our quantitative analysis of immunofluorescence in numerous sections showed a gradual increase in the vessel diameter over time after dual cell transplantation, supporting continuous remodeling of the initially regenerated artery or arterioles to larger ones. The large artery with a diameter > 50 μm was frequently detected at 12 weeks of dual cell transplantation but only small vessels < 15 μm in diameter were detected in remaining tissues in the saline group, strongly suggesting that small vessels can be generated from endogenous capacity but is clearly insufficient and limited for limb salvage. This necessitates the therapeutic adoption of ex vivo cultured dual cells for immediate arterial restoration in patients with severe CLI. Considering that mouse arteries are much smaller than human arteries [33], the large vessel seen macroscopically at day 7 of dual cell transplantation may be restored concomitantly by bridging existing collaterals and active participation of transplanted dual cells. The angiogenic paracrine effect of VPCs and BM-MSCs on endogenous arteriogenesis was also considered.

Most tissues comprise multiple cell types that cooperate and regulate each other for unique tissue functions by sharing paracrine factors, ECMs, and direct cell–cell communication through adhesion. Thus, combination cell therapy comprising multiple functional cells may be essential for tissue repair. However, most cell therapies have been attempted using singular cell type, whose engraftment and efficacy have been much lower than expected and have not been consistently validated. In particular, blood vessels are composed of different cell layers with unique functions. Capillaries in a variety of tissues are composed of inner lining ECs and outer encircling pericytes in different cell ratios. Arterioles and arteries are also composed of inner lining ECs and thick VSMC media layer depending on the vessel diameter. Transplantation of VPCs and BM-MSCs into a superficial femoral artery-excised CLI model showed restoration of arteries or arterioles, blood flow recovery, and limb salvage, unless limb loss occurred. In addition, dual cell therapy was more effective than singular transplantation at the same cell dose, strongly supporting the idea that the two cell types work synergistically in vascular repair. Their fate confirmation also supports the adoption of two cell fates by the transplanted cells, in which VPCs may adopt the human endothelial phenotype, and BM-MSCs may become either human pericytes or smooth muscle cells under in vivo environment of CLI. However, another possibility of conversion of VPCs to human α-SMA-expressing VSMCs or conversion of BM-MSCs to human CD31-expressing ECs exists but could not be proven in this study. Nevertheless, the cell fate in singular transplantation supports the human endothelial fate of VPCs and the human VSMC fate of BM-MSCs.

Conclusions

Collectively, this is the first evidence showing the restoration of the large artery and limb salvage with $CD141^+$VPC and BM-MSC dual cell therapy in a 2:1 ratio as a reparative cell therapy in a severe CLI model, which is expected to be used clinically for severe PAD and other ischemic vascular diseases.

Abbreviations

α-SMA	Alpha-smooth muscle actin
BM	Bone marrow
BMA	Bone marrow aspirates
CB	Cord blood
CLI	Critical limb ischemia
ECFCs	Endothelial colony forming cells
EPCs	Endothelial precursor cells
HGF	Hepatocyte growth factor
hPL	Human platelet lysate
HUVECs	Human umbilical cord vein endothelial cells
MSC	Mesenchymal stem cells
PAD	Peripheral artery disease
PB	Peripheral blood
PDT	Population doubling time
TAGLN	Transgelin
TNF-α	Tumor necrosis factor-alpha
UEA-1	Ulex europaeus agglutinin-1
VEGF	Vascular endothelial growth factor
VESCs	Vascular endothelial stem cells

VPCs	Vasculogenic precursor cells
VSMCs	Vascular smooth muscle cells
vWF	Von willebrand factor
WGA	Wheat germ agglutinin

Supplementary Information

The online version contains supplementary material available at https://doi.org/10.1186/s13287-024-03994-9.

Additional file 1.

Acknowledgements
The authors declare that they have not used Artificial Intelligence in this study.

Author contributions
Conceptualization, Y.S., H.S.H, Formal analysis: GP, DYH, HSH, DYK, Investigation: GP, DYH, DYK, JSP, JYH, EL, HH, DWK, SMH, Writing-original draft: YS, HSH, Writing-review and editing: YS. Visualization: GP, DYH, HSH, DYK, Project administration: YS, SVY, HSH, Funding acquisition, YS, SVY, HSH.

Funding
This study was supported by a Korean Health Technology R&D Project grant (HI18C1492) from the Ministry of Health and Welfare (Sejong, Republic of Korea), by Korean Fund for Regenerative Medicine (KFRM) grant funded by the Korea government (the Ministry of Science and ICT, the Ministry of Health & Welfare), (23C0110L1) and by Research fund by Elphis Cell Therapeutics.

Availability of data and materials
The datasets used and/or analyzed during the current study are available from the corresponding author on reasonable request.

Declarations

Ethics approval and consent to participate
(1) Animal experiment for the efficacy of dual stem cell in limb ischemia (2) The Ethics Committee for Experimental Animals of Kyung Hee University Hospital (3) KHMC-IACUC 20-008 (4) 2021.3.11. The protocols for animal experiments adhere to the ARRIVE (Animal Research: Reporting of in Vivo Experiments) guidelines. (1) Fresh BM of human was obtained from donors for effectiveness of stem cell therapy (2) The Institutional Review Board of Kyung Hee University hospital (3) 2020-09-036 (4) 2020.10.23 Patient provided written informed consent for the use of samples. Human BM-MNCs, frozen manufactured by Lonza were isolated from donated human tissue after obtaining permission for their use in research applications by informed consent or legal authorization. Human BM-MNCs frozen manufactured by STEMCELL Technologies were obtained using Institutional Review Board (IRB) approved consent forms and protocols.

Consent for publication
All authors confirm their consent for publication.

Competing interests
All authors declare that they have no conflicts of interes.t

Author details
[1]R&D Center, Elphis Cell Therapeutics Inc, Yong In 17095, Korea. [2]Department of Biomedical Science and Technology, Graduated School, Kyung Hee University, Seoul, Korea. [3]Department of Genetic Engineering, Graduate School of Biotechnology, Kyung Hee University, Yong In, Korea. [4]Department of Clinical Pharmacology and Therapeutics, College of Medicine, Kyung Hee University, Seoul, Korea. [5]East-West Medical Research Institute, Kyung Hee University, Seoul, Korea.

Received: 9 July 2024 Accepted: 10 October 2024
Published online: 31 October 2024

References

1. Asahara T, Murohara T, Sullivan A, Silver M, van der Zee R, Li T, Witzenbichler B, Schatteman G, Isner JM. Isolation of putative progenitor endothelial cells for angiogenesis. Science. 1997;275(5302):964–6.
2. Chambers SE, Pathak V, Pedrini E, Soret L, Gendron N, Guerin CL, Stitt AW, Smadja DM, Medina RJ. Current concepts on endothelial stem cells definition, location, and markers. Stem Cells Transl Med. 2021;10(S2):S54–61.
3. Yoder MC. Endothelial stem and progenitor cells (stem cells):(2017 Grover Conference Series). Pulm Circ. 2017;8(1):2045893217743950.
4. Medina RJ, O'Neill CL, Sweeney M, Guduric-Fuchs J, Gardiner TA, Simpson DA, Stitt AW. Molecular analysis of endothelial progenitor cell (EPC) subtypes reveals two distinct cell populations with different identities. BMC Med Genomics. 2010;3:1–13.
5. Minami Y, Nakajima T, Ikutomi M, Morita T, Komuro I, Sata M, Sahara M. Angiogenic potential of early and late outgrowth endothelial progenitor cells is dependent on the time of emergence. Int J Cardiol. 2015;186:305–14.
6. Fujisawa T, Tura-Ceide O, Hunter A, Mitchell A, Vesey A, Medine C, Gallogly S, Hadoke PW, Keith C, Sproul A. Endothelial progenitor cells do not originate from the bone marrow. Circulation. 2019;140(18):1524–6.
7. Yu QC, Song W, Wang D, Zeng YA. Identification of blood vascular endothelial stem cells by the expression of protein C receptor. Cell Res. 2016;26(10):1079–98.
8. Wakabayashi T, Naito H, Suehiro J-i, Lin Y, Kawaji H, Iba T, Kouno T, Ishikawa-Kato S, Furuno M, Takara K. CD157 marks tissue-resident endothelial stem cells with homeostatic and regenerative properties. Cell Stem Cell. 2018;22(3):384–97.
9. Zemaitis MR, Boll JM, Dreyer MA: Peripheral arterial disease. 2017.
10. Kawamoto A, Katayama M, Handa N, Kinoshita M, Takano H, Horii M, Sadamoto K, Yokoyama A, Yamanaka T, Onodera R. Intramuscular transplantation of G-CSF-mobilized CD34+ cells in patients with critical limb ischemia: a phase I/IIa, multicenter, single-blinded, dose-escalation clinical trial. Stem Cells. 2009;27(11):2857–64.
11. Idei N, Soga J, Hata T, Fujii Y, Fujimura N, Mikami S, Maruhashi T, Nishioka K, Hidaka T, Kihara Y. Autologous bone-marrow mononuclear cell implantation reduces long-term major amputation risk in patients with critical limb ischemia: a comparison of atherosclerotic peripheral arterial disease and Buerger disease. Circ Cardiovasc Intervent. 2011;4(1):15–25.
12. Qadura M, Terenzi DC, Verma S, Al-Omran M, Hess DA. Concise review: cell therapy for critical limb ischemia: an integrated review of preclinical and clinical studies. Stem Cells. 2018;36(2):161–71.
13. Raval Z, Losordo DW. Cell therapy of peripheral arterial disease: from experimental findings to clinical trials. Circ Res. 2013;112(9):1288–302.
14. Annex BH, Cooke JP. New directions in therapeutic angiogenesis and arteriogenesis in peripheral arterial disease. Circ Res. 2021;128(12):1944–57.
15. Huang NF, Stern B, Oropeza BP, Zaitseva TS, Paukshto MV, Zoldan J. Bioengineering cell therapy for treatment of peripheral artery disease. Arterioscler Thromb Vasc Biol. 2024;44(3):e66–81.
16. Dar A, Domev H, Ben-Yosef O, Tzukerman M, Zeevi-Levin N, Novak A, Germanguz I, Amit M, Itskovitz-Eldor J. Multipotent vasculogenic pericytes from human pluripotent stem cells promote recovery of murine ischemic limb. Circulation. 2012;125(1):87–99.
17. Park JJ, Kwon YW, Kim JW, Park GT, Yoon JW, Kim YS, Kim DS, Kwon SM, Bae SS, Ko K. Coadministration of endothelial and smooth muscle cells derived from human induced pluripotent stem cells as a therapy for critical limb ischemia. Stem Cells Transl Med. 2021;10(3):414–26.
18. MacAskill MG, Saif J, Condie A, Jansen MA, MacGillivray TJ, Tavares AA, Fleisinger L, Spencer HL, Besnier M, Martin E. Robust revascularization in models of limb ischemia using a clinically translatable human stem cell-derived endothelial cell product. Mol Ther. 2018;26(7):1669–84.
19. Park SY, Lee H, Kwon YW, Park MR, Kim JH, Kim JB. Etv2-and fli1-induced vascular progenitor cells enhance functional recovery in ischemic vascular disease model—brief report. Arterioscler Thromb Vasc Biol. 2020;40(4):e105–13.
20. Bergers G, Song S. The role of pericytes in blood-vessel formation and maintenance. Neuro Oncol. 2005;7(4):452–64.
21. Paschalaki KE, Randi AM. Recent advances in endothelial colony forming cells toward their use in clinical translation. Front Med. 2018;5:295.
22. Attwood SW, Edel MJ. iPS-cell technology and the problem of genetic instability—Can it ever be safe for clinical use? J Clin Med. 2019;8(3):288.

23. Popescu S, Preda MB, Marinescu CI, Simionescu M, Burlacu A. Dual stem cell therapy improves the myocardial recovery post-infarction through reciprocal modulation of cell functions. Int J Mol Sci. 2021;22(11):5631.
24. Tamama K, Sen CK, Wells A. Differentiation of bone marrow mesenchymal stem cells into the smooth muscle lineage by blocking ERK/MAPK signaling pathway. Stem Cells Dev. 2008;17(5):897–908.
25. Kim S, Lee S, Lim J, Choi H, Kang H, Jeon NL, Son Y. Human bone marrow-derived mesenchymal stem cells play a role as a vascular pericyte in the reconstruction of human BBB on the angiogenesis microfluidic chip. Biomaterials. 2021;279: 121210.
26. Loghmani H, Conway EM. Exploring traditional and nontraditional roles for thrombomodulin. Blood J Am Soc Hematol. 2018;132(2):148–58.
27. Kuo C-H, Huang Y-H, Chen P-K, Lee G-H, Tang M-J, Conway EM, Shi G-Y, Wu H-L. VEGF-induced endothelial podosomes via ROCK2-dependent thrombomodulin expression initiate sprouting angiogenesis. Arterioscler Thromb Vasc Biol. 2021;41(5):1657–71.
28. Xu Y, Zhou Y, Lin H, Hu H, Wang Y, Xu G. Toll-like receptor 2 in promoting angiogenesis after acute ischemic injury. Int J Mol Med. 2013;31(3):555–60.
29. Talele NP, Fradette J, Davies JE, Kapus A, Hinz B. Expression of α-smooth muscle actin determines the fate of mesenchymal stromal cells. Stem Cell Rep. 2015;4(6):1016–30.
30. Tsuji-Tamura K, Morino-Koga S, Suzuki S, Ogawa M. The canonical smooth muscle cell marker TAGLN is present in endothelial cells and is involved in angiogenesis. J Cell Sci. 2021;134(15):jcs254920.
31. Dominici M, Le Blanc K, Mueller I, Slaper-Cortenbach I, Marini F, Krause D, Deans R, Keating A, Prockop D, Horwitz E. Minimal criteria for defining multipotent mesenchymal stromal cells. The International Society for Cellular Therapy position statement. Cytotherapy. 2006;8(4):315–7.
32. Bussolino F, Di Renzo MF, Ziche M, Bocchietto E, Olivero M, Naldini L, Gaudino G, Tamagnone L, Coffer A, Comoglio P. Hepatocyte growth factor is a potent angiogenic factor which stimulates endothelial cell motility and growth. J Cell Biol. 1992;119(3):629–41.
33. Müller B, Lang S, Dominietto M, Rudin M, Schulz G, Deyhle H, Germann M, Pfeiffer F, David C, Weitkamp T: High-resolution tomographic imaging of microvessels. In: *Developments in X-ray tomography VI: 2008*: SPIE; 2008: 89–98.
34. Nair AB, Jacob S. A simple practice guide for dose conversion between animals and human. J Basic Clin Pharm. 2016;7(2):27.
35. Lee HC, An SG, Lee HW, Park J-S, Cha KS, Hong TJ, Park JH, Lee SY, Kim S-P, Kim YD. Safety and effect of adipose tissue-derived stem cell implantation in patients with critical limb ischemia–a pilot study. Circ J. 2012;76(7):1750–60.
36. Swaminathan A, Vemulapalli S, Patel MR, Jones WS: Lower extremity amputation in peripheral artery disease: improving patient outcomes. *Vascular health and risk management* 2014:417–424.
37. Bray LJ, Heazlewood CF, Atkinson K, Hutmacher DW, Harkin DG. Evaluation of methods for cultivating limbal mesenchymal stromal cells. Cytotherapy. 2012;14(8):936–47.
38. Kim DY, Park G, Hong HS, Kim S, Son Y. Platelet-derived growth factor-bb priming enhances vasculogenic capacity of bone marrow-derived endothelial precursor like cells. Tissue Eng Regen Med. 2023;20(5):695–704.
39. Shi X, Zhang W, Yin L, Chilian WM, Krieger J, Zhang P. Vascular precursor cells in tissue injury repair. Transl Res. 2017;184:77–100.
40. Dight J, Zhao J, Styke C, Khosrotehrani K, Patel J: Resident vascular endothelial progenitor definition and function: the age of reckoning. *Angiogenesis* 2022:1–19.
41. Jang HH, Son Y, Park G, Park K-S. Bone marrow-derived vasculogenic mesenchymal stem cells enhance in vitro angiogenic sprouting of human umbilical vein endothelial cells. Int J Mol Sci. 2022;24(1):413.
42. Jiang W, Xu J. Immune modulation by mesenchymal stem cells. Cell Prolif. 2020;53(1): e12712.
43. Qin Q, Qian J, Ge L, Shen L, Jia J, Jin J, Ge J. Effect and mechanism of thrombospondin-1 on the angiogenesis potential in human endothelial progenitor cells: an in vitro study. PLoS ONE. 2014;9(2): e88213.
44. Smadja DM, d'Audigier C, Bieche I, Evrard S, Mauge L, Dias J-V, Labreuche J, Laurendeau I, Marsac B, Dizier B. Thrombospondin-1 is a plasmatic marker of peripheral arterial disease that modulates endothelial progenitor cell angiogenic properties. Arterioscler Thromb Vasc Biol. 2011;31(3):551–9.
45. Hirschi KK, Ingram DA, Yoder MC. Assessing identity, phenotype, and fate of endothelial progenitor cells. Arterioscler Thromb Vasc Biol. 2008;28(9):1584–95.
46. Iruela-Arispe ML, Lombardo M, Krutzsch HC, Lawler J, Roberts DD. Inhibition of angiogenesis by thrombospondin-1 is mediated by 2 independent regions within the type 1 repeats. Circulation. 1999;100(13):1423–31.
47. Van Royen N, Piek JJ, Buschmann I, Hoefer I, Voskuil M, Schaper W. Stimulation of arteriogenesis; a new concept for the treatment of arterial occlusive disease. Cardiovasc Res. 2001;49(3):543–53.

Publisher's Note